HOKKAIDO UNIVERSITY

Title	Study of the function of pallial to basal ganglia projecting neurons in vocal learning and maintenance in songbirds
Author(s)	SANCHEZ VALPUESTA, MIGUEL
Degree Grantor	北海道大学
Degree Name	博士(生命科学)
Dissertation Number	甲第13952号
Issue Date	2020-03-25
DOI	https://doi.org/10.14943/doctoral.k13952
Doc URL	https://hdl.handle.net/2115/78054
Type	doctoral thesis
File Information	SANCHEZ_VALPUESTA_MIGUEL.pdf

Hokkaido University Collection of Scholarly and Academic Papers : HUSCAP

Study of the function of pallial to basal ganglia projecting neurons in vocal learning and maintenance in songbirds

（鳴禽類の外套−基底核投射ニューロンの発声学習、及び維持における神経機能の研究）

A DISSERTATION

Submitted to the Graduate School of Life Science,

Hokkaido University

In partial fulfilment of the requirements for award of the degree

DOCTOR OF LIFE SCIENCE

Miguel Sánchez-Valpuesta

March, 2020

Contents

Introduction 3

Materials and Methods 19

Results 37

Discussion 68

Acknowledgements 73

References 75

Main Publication 86

List of other publications 87

Introduction

Many of our commonly used skills, like speech, writing or even playing music are acquired during a long period of motor practice matching the subject's initially poor motor skills to a previously learned model (Tanji, 2001; Hikosaka et al., 2002). A simple example of motor skill learning is motor sequence learning (Kornysheva, 2016; Garr, 2019). Over the course of experimental motor sequence learning in primates, neuronal firing in prefrontal cortical areas develops firing patterns locked to the boundaries of motor sequences, such as start and stop signals (Fujii and Graybiel, 2013). This firing locked to movement sequence boundaries not only develops in the prefrontal cortex, but it also develops downstream in the basal ganglia (Barnes et al., 2005). The cortical to basal ganglia connections mediating this transfer are thought to be important for the transfer of general motor timing information into the basal ganglia (Jin and Costa, 2010). However, the natural learning of many motor skills is guided by internal goals instead of external reward as in training experiments. Studies in sensorimotor learning settings indicate that motor learning from internal goals is more closely related to the function of motor cortices (Shadmehr and Krakauer, 2008). However, precisely how the motor, instead of prefrontal executive, cortices contribute mechanistically to motor skill learning remains still largely unknown. Motor cortical areas in primate brains develop neuronal firing time-locked to ongoing movements and not just sequence boundaries during learning, especially in their basal ganglia-projecting deep layers (Li et al., 2017). This time-locked input has been hypothesized to be crucial for the learning, execution and evaluation of motor acts (Fee and Goldberg, 2011; Tesileanu et al., 2017). Furthermore, plasticity at cortical to basal ganglia synapses has been related to the

learning of motor sequences (Jin and Costa, 2010; Koralek et al., 2012), with corticostriatal plasticity being involved in motor pathologies (Warre et al., 2011; Madeo et al., 2012). Therefore, a deeper understanding of the roles of motor cortical input into the basal ganglia for motor skill learning will be of value for basic neuroscience and also towards the understanding of motor pathologies (Stefanova et al., 2000; Willingham and Koroshetz, 1993).

However, investigating the involvement of corticobasal neurons in motor skill learning using mammalian models is a difficult task. Rodents are powerful models at the neuronal level but show poor skill learning. Primates are powerful at the behavioral level but are difficult to breed and experiment with at the molecular neuronal level. Therefore, an avian model, the zebra finch was used in this study. Most oscine songbirds learn their adult songs during a protracted process of motor skill learning known as vocal learning (Konishi, 1965; Marler, 1970). Other animals like suboscine songbirds or marmosets undergo a protracted development of fundamentally innate vocalizations (Liu et al., 2013; Takahashi et al., 2017). Oscine songbirds memorize their tutor's song, learning how to imitate it through a series of stages involving sensory feedback and motor practice (**Figure I-1**). This vocal learning process possesses two advantages to study motor skill learning, first it resembles the most the learning of speech in human infants (Doupe and Kuhl, 1999). Secondly, it depends on a well characterized set of brain regions dedicated to the learning and production of birdsong, the song system (Brenowitz et al., 1997; Jarvis, 2004). This song system is formed by two pathways of interconnected nuclei, the posterior vocal motor pathway (VMP) and the anterior forebrain pathway (AFP) (**Figure I-2*A***). The VMP is necessary to produce adult birdsong, while the AFP is necessary for juvenile song learning (Bottjer et al.,

1984; Sohrabji et al., 1990; Scharff and Nottebohm, 1991). The VMP is composed of nucleus HVC (used as a proper name) projecting to nucleus robustus of the arcopallium (RA), a cortical layer 5-like nucleus that drives the of the syrinx-innervating hypoglossal nucleus (nXIIts) (Vicario and Nottebohm, 1988; Wild, 1993). Conversely, the AFP is formed by a basal ganglia-thalamo-pallium (cortical) loop spanning three nuclei, the basal ganglia Area X, the medial part of the dorsolateral thalamic nucleus (DLM) and the cortical-like lateral part of the magnocellular nucleus of the anterior nidopallium (LMAN). The AFP finally converges on the vocal motor pathway through LMAN's synapses on nucleus RA.

Cortical-like nucleus HVC contains two different kinds of projection neurons: $HVC_{(RA)}$ neurons projecting to nucleus RA-and $HVC_{(X)}$ neurons projecting to the AFP basal ganglia nucleus Area X (Dutar et al., 1998; Kubota and Taniguchi, 1998) (**Figure I-2*B***). During song learning, both populations of projection neurons in nucleus HVC develop a chain-like firing pattern (Hahnloser et al., 2002; Long et al., 2010; Okubo et al., 2015; Lynch et al., 2016). This firing pattern is composed at the individual neuron level of precise time-locked bursts to specific time points in the bird's song motifs. This development of time-locked firing is reminiscent of the rough movement-locked firing pattern of mammalian motor cortical neurons, which becomes more time-locked during motor skill learning (Turner and DeLong, 2000; Li et al., 2017). Thus, bursts sparsely locked to specific times during the whole song are available to Area X neurons through synapses arising from $HVC_{(X)}$ neurons. However, the function of time-locked $HVC_{(X)}$ input to the Area X still remains unknown. Hints from song learning mechanisms suggested by several hypotheses can help answering this question.

There exist different hypotheses concerning the role of $HVC_{(X)}$ input into the basal ganglia in vocal learning. An early hypothesis suggested that the AFP and the $HVC_{(X)}$ neurons were involved in computing auditory feedback signals for learning (Solis et al., 2000). However, recent electrophysiological work contested this hypothesis after finding that HVC neurons are mostly unresponsive to auditory information in the awake condition (Hamaguchi et al., 2014; Vallentin and Long, 2015; Picardo et al., 2016). An alternative hypothesis based on a reinforcement learning framework has been recently suggested for the function of $HVC_{(X)}$ input into the basal ganglia in vocal learning (Fee and Goldberg, 2011). According to this hypothesis, the role of the AFP is to inject vocal variability into the VMP that will later be adaptively selected through an auditory feedback-dependent process to render a song progressively more similar to the tutor. Area X and the whole AFP loop is composed of a series of parallel channels that affect the song in different ways (increasing or lowering pitch, stopping the song, etc.) and are randomly activated at the beginning of learning. Conversely, $HVC_{(X)}$ neurons fire time-locked bursts temporally covering the whole song in an ordered fashion. The goal of the reinforcement learning mechanism lies in correctly wiring the $HVC_{(X)}$ neurons corresponding to every song time point to the correct AFP channels, thus driving down song variability and producing a song more similar to the tutor (**Figure I-3*A***). However, the actual function of $HVC_{(X)}$ neurons has not been examined in the context of a reinforcement learning framework.

In short, the reinforcement learning model works as follows (Fee and Goldberg, 2011). Neural activity starting from an Area X neuron population in a parallel channel active at a certain time point in the song will flow through the AFP circuit and return exactly onto the same Area X neuron population (Luo et al., 2001). In this way a copy of the

signal sent to RA neurons by LMAN neurons returns to the same Area X neurons that generated it. Area X neurons thus obtain three important signals to drive song learning. The first signal would be time-locked input from $HVC_{(X)}$ neurons providing "temporal context" information about the current temporal location inside the song. The second signal would be LMAN input conveying a "variability copy" that corresponds to the variability injected to the VMP at the $HVC_{(X)}$-specified time point. Finally, the third signal would be an "evaluative input" from Area X-projecting Ventral Tegmental Area (VTA neurons) indicating whether vocal motor performance at the $HVC_{(X)}$-specified time point was better or worse when compared to the tutor song memory (Gadagkar et al., 2016; Hisey et al., 2018). Each $HVC_{(X)}$ neuron sends temporal context information corresponding to a specific song time point to a population of Area X medium spiny neurons. Whether the corticobasal synapse linking the specific temporal context, conveyed by $HVC_{(X)}$ input, to the vocal motor change caused by the specific Area X neuron population is potentiated depends on dopamine release by VTA neurons. Dopaminergic axons in Area X increase dopamine release whether the song produced is more similar to the tutor (Fee and Goldberg, 2011). This process progressively wires $HVC_{(X)}$ neurons representing every time step in the song to the Area X neurons producing the best sounding output, thus increasing the acoustic similarity to the tutor. However, the validity of the reinforcement learning model rests on the expectation that time-locked $HVC_{(X)}$ input is indeed used to "wire" the correct AFP variability-generating channels to the correct time points in the song. The removal of $HVC_{(X)}$ neurons can thus be predicted to affect the learning of tutor songs by failing to reduce the variability fed into the final song by the AFP. This could cause several effects on the

final song of $HVC_{(X)}$ neuron-ablated birds, such as a failure to crystallize acoustics or sequence in a fixed motif.

Furthermore, adult zebra finches still retain a significant ability to adaptively modify their own song's acoustics. This ability can be revealed by several studies training adult zebra finches to shift up or down the pitch of their songs through aversive conditioning (Sober and Brainard, 2009; Ali et al., 2013, Xiao et al., 2018). Another way to uncover this ability of adult songbirds to modify their own song is by presenting the adult songbird with distorted auditory feedback of its own song, which causes a gradual decrystallization (Leonardo and Konishi, 1999; Fukushima and Margoliash, 2015). The capacity of adult songbirds to modify their vocal motor output after sensory manipulation or disruption is reminiscent to the human capacity to adaptively modify the acoustic properties of speech under sensory feedback distortion (Liu et al., 2010; Feng et al., 2018). This plasticity may serve similar functions in songbirds for the active adaptation of vocal output not just to motor errors, but also to counter ambient noise conditions and acoustic distortion (Patricelli and Blickley, 2006; Slabbekoorn and Ripmeester, 2007). Although the origin of these adaptive vocal abilities in humans is still obscure, in songbirds the neuroanatomy behind the ability to modify adult birdsong is better known. Pitch-shift conditioning in adult birds requires intact Area X and LMAN nuclei (Kao et al., 2005; Ali et al., 2013). Likewise, optogenetic stimulation of VTA can drive pitch shifting in zebra finch adults (Xiao et al., 2018). Therefore, AFP nuclei are innervated by $HVC_{(X)}$ neurons, which suggests a possible role of time-locked $HVC_{(X)}$ input into the basal ganglia in adult song maintenance. However, this potential role of $HVC_{(X)}$ neurons in adult song maintenance has not been fully elucidated yet.

A direct way to experimentally test the degree of adult vocal plasticity and its role in vocal maintenance is through deafening-induced song degradation (Leonardo and Konishi, 1999; Horita et al., 2008). Young adult zebra finches display a progressive loss of their acquired song acoustics and sequence after deafening, putatively because their ability to match their motor output to the heard sensory feedback input is completely lost after deafening, causing aberrant dopamine input to the AFP reinforcement learning circuit. Experimentally lesioning Area X before deafening in young adult zebra finches prevents deafening-induced song degradation while abolishing LMAN burst firing (Kojima et al., 2013), decisively implicating Area X in song maintenance and indicating that AFP-caused vocal fluctuations may play a role in vocal plasticity. A more recent study confirmed that within-syllable vocal fluctuations in fundamental frequency (FF) selected for in pitch shifting were abolished by Area X lesions (Kojima et al., 2018). $HVC_{(X)}$ neurons are thought to provide not just the time-locked "context" information needed for the reinforcement learning hypothesized to lie behind the adult plasticity phenomena mentioned above, but also are one of the main driving excitatory inputs of Area X medium spiny neurons and pallidal-like neurons (Pidoux et al., 2015). However, despite many studies relating the function of the AFP to adult song maintenance and the likely role of $HVC_{(X)}$ neurons in this mechanism due to neuroanatomy, a previous $HVC_{(X)}$ neuron ablation study in adults found no large-scale effects on song (Scharff et al., 2000). Whether $HVC_{(X)}$ neurons play any role in adult song maintenance remains to be assessed by using more sensitive behavioral tests after $HVC_{(X)}$ neuron ablation.

Additionally, from an evolutionary viewpoint, vocal learning bird clades where neuroanatomy has been well traced also support a function for motor cortical-like projections to the basal ganglia in vocal learning. Both oscine songbirds and parrots

possess projections to the basal ganglia originating from their song premotor circuits. In oscine songbirds these are the previously mentioned $HVC_{(X)}$ neurons, in parrots and budgerigars projections to the basal ganglia nucleus medial magnocellular striatum (MMSt) arise similarly from both cortical-like central nucleus of lateral nidopallium (NLC) and central nucleus of the anterior arcopallium (AAC) (Striedter, 1994; Chakraborty et al., 2015). This anatomical disposition not just exists in a parallel way in two separated vocal learning clades, but in the non-vocal learning songbird where connectivity has been studied, the eastern phoebe (*Sayornis phoebe*), a VMP could be found but no vocalization-related cortical-basal ganglia projecting pathway exists (Liu et al., 2013). The absence of motor cortical-like to basal ganglia projections from vocalization-related areas in non-vocal learners suggests that motor cortical to basal ganglia projections are crucial for vocal learning and may be related to its evolution (**Figure I-3**).

The purpose of this study is to elucidate the function of $HVC_{(X)}$ neurons in songbird vocal learning at the juvenile stage and in song maintenance at the adult stage. To test the functions of this neuron population, $HVC_{(X)}$ neurons were ablated in a cell type-specific manner using viral tools at the juvenile and adult stages and their behavior carefully monitored and analyzed.

Figure I-1

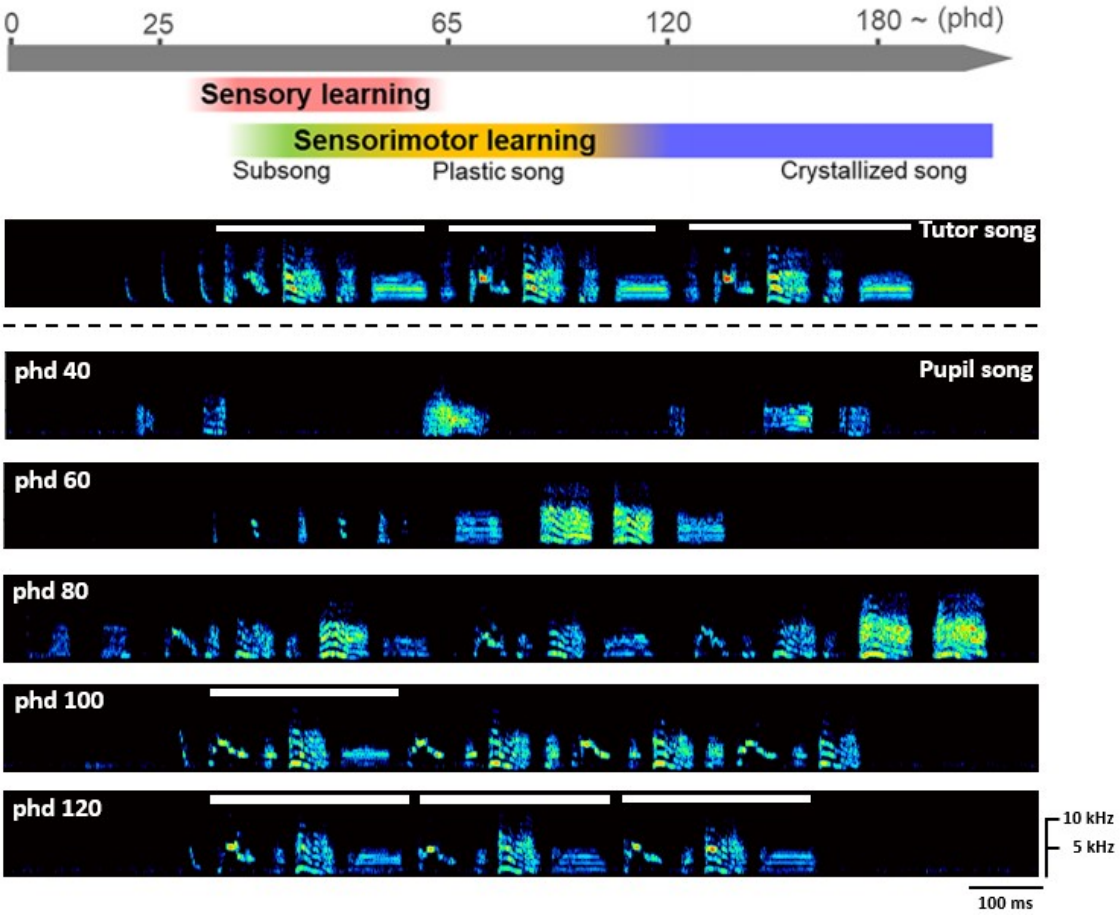
0
25
65
120
180 ~ (phd)
Sensory learning
Sensorimotor learning
Subsong
Plastic song
Crystallized song
Tutor song
phd 40
Pupil song
phd 60
phd 80
phd 100
phd 120
10 kHz
5 kHz
100 ms

Sonograms of zebra finch song development along the critical period of vocal learning. White bars represent the motif structure of the crystallized song.

Figure I-2

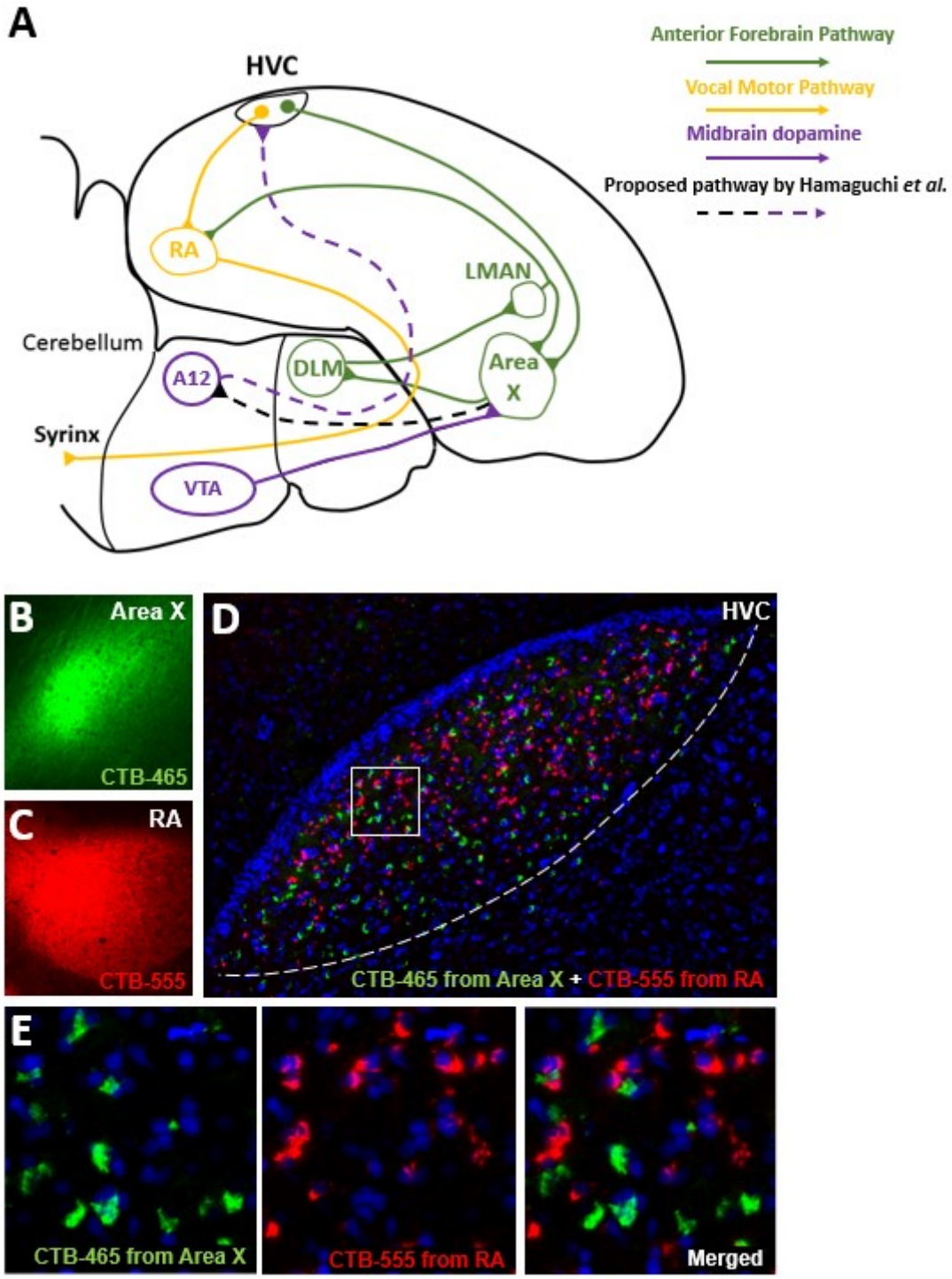
A
HVC
Anterior Forebrain Pathway
Vocal Motor Pathway
Midbrain dopamine
Proposed pathway by Hamaguchi *et al.*
RA
LMAN
Cerebellum
A12
DLM
Area X
Syrinx
VTA
B
Area X
CTB-465
C
RA
CTB-555
D
HVC
CTB-465 from Area X + CTB-555 from RA
E
CTB-465 from Area X
CTB-555 from RA
Merged

A) Diagram showing selected song-control brain regions and connections in the zebra finch brain. The posterior motor pathway and the anterior forebrain pathway (cortical-basal ganglia-thalamic circuit) are represented as yellow and green lines, respectively. The dopaminergic pathway from midbrain neurons is represented by a purple line. HVC (used as a proper name); RA, the robust nucleus of the arcopallium; Area X, Area X of the basal ganglia; DLM, dorsal lateral nucleus of the medial thalamus; LMAN, lateral magnocellular nucleus of the anterior nidopallium; NIf, interfacial nucleus of the nidopallium; nXIIts, tracheosyringeal part of the hypoglossal nucleus. VTA, ventral tegmental area.

B) Injection point of retrograde tracer Cholera Toxin B (CTB) -465 in Area X.

C) Injection point of retrograde tracer CTB-555 in nucleus RA.

D) Full nucleus view of HVC with both $HVC_{(X)}$ neurons labeled in green by retrograde tracer from Area X and $HVC_{(RA)}$ neurons labeled in red from nucleus RA.

E) Inset from **D)** showing that both $HVC_{(X)}$ and $HVC_{(RA)}$ neurons belong to segregated populations.

Figure I-3

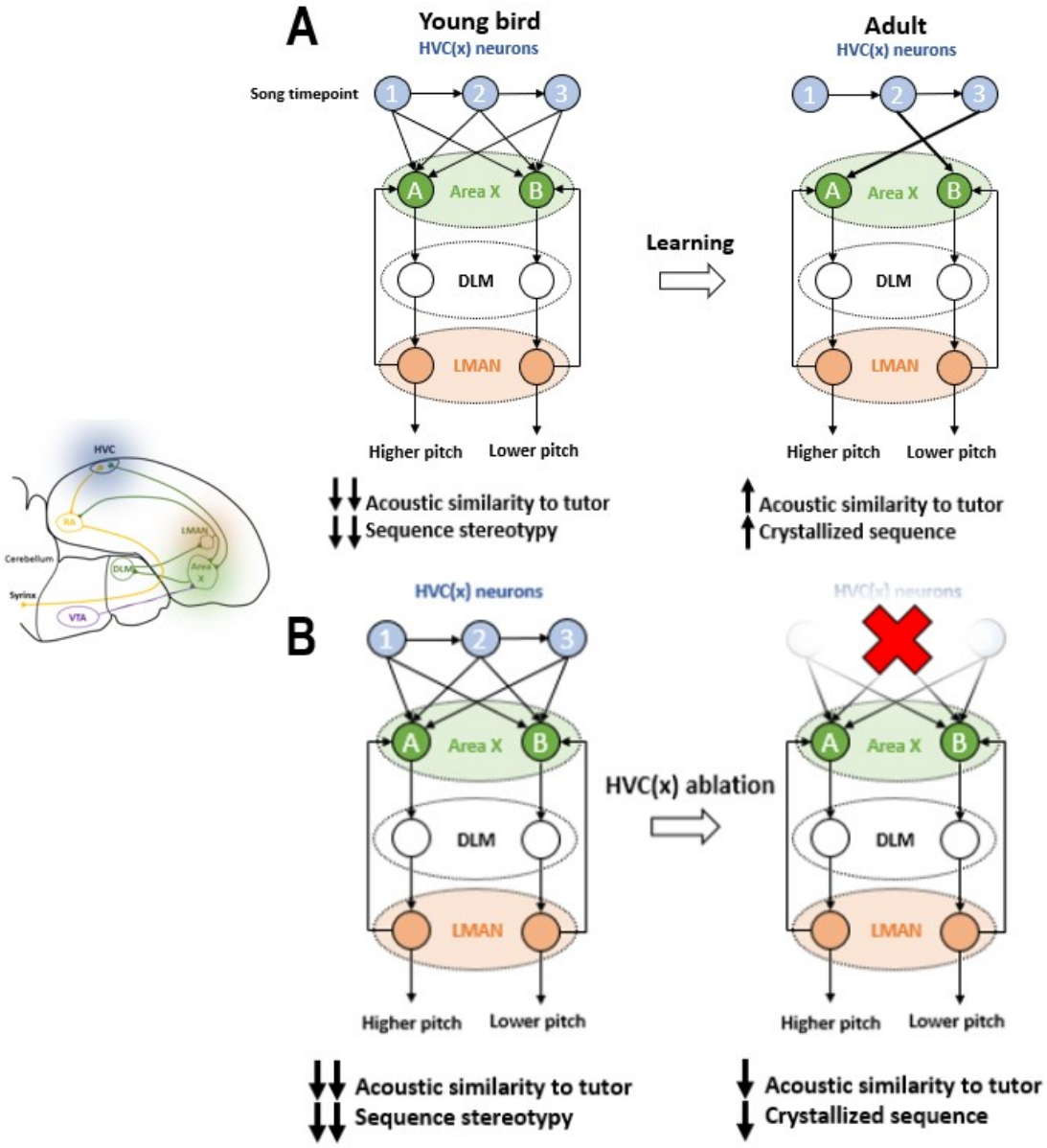
A
Young bird
HVC(x) neurons
Song timepoint
1
2
3
A
Area X
B
DLM
LMAN
Higher pitch
Lower pitch
Learning
Adult
HVC(x) neurons
Acoustic similarity to tutor
Sequence stereotypy
Acoustic similarity to tutor
Crystallized sequence
HVC
RA
LMAN
Cerebellum
DLM
Area X
Syrinx
VTA
B
HVC(x) neurons
HVC(x) ablation
Acoustic similarity to tutor
Sequence stereotypy
Acoustic similarity to tutor
Crystallized sequence

A) Schematic representation of the reinforcement learning model for the function of the AFP. In the intact bird, the blue circles represent the sequential time-locked firing of $HVC_{(X)}$ neurons along the bird's own song. The green, white and orange circles represent Area X, DLM and LMAN cell populations, respectively. These populations are segregated into many parallel AFP channels, represented in this diagram by the two channels denoted as "A" and "B". At the beginning of the learning, $HVC_{(X)}$ neurons representing different time points connect non-specifically to many parallel AFP channels. Over learning, the specific song time points represented by $HVC_{(X)}$ neurons are "wired" to specific AFP channels, causing more and more restricted AFP-driven changes at each song time point.

B) Hypothesized effects of $HVC_{(X)}$ ablation on song learning and production. After ablation of most $HVC_{(X)}$ neurons, the different AFP channels cannot be correctly "wired" to the specific time points marked by $HVC_{(X)}$ neuron firing. This could cause an inability to crystallize the adult song sequence and a failure of the juvenile bird to correctly copy the tutor acoustics, due to the reduced ability to wire each time point to the correct AFP channels.

Figure I-4

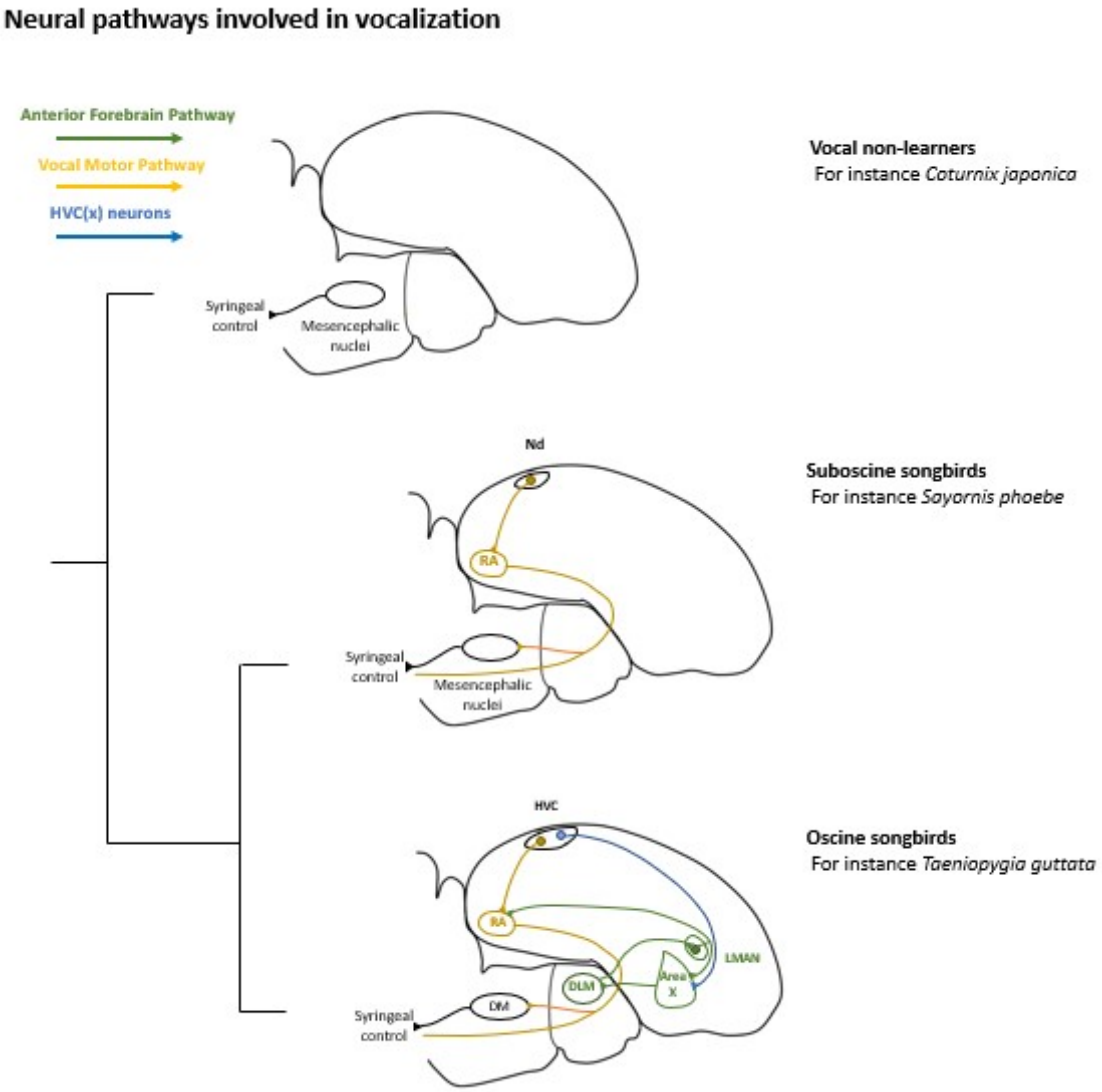
Neural pathways involved in vocalization
Anterior Forebrain Pathway
Vocal Motor Pathway
HVC(x) neurons
Syringeal control
Mesencephalic nuclei
Vocal non-learners
For instance Coturnix japonica
Nd
RA
Syringeal control
Mesencephalic nuclei
Suboscine songbirds
For instance Sayornis phoebe
HVC
RA
LMAN
Area X
DLM
DM
Syringeal control
Oscine songbirds
For instance Taeniopygia guttata

Neuroanatomical differences in song learning and song learning pathways in vocal learning songbirds and non-vocal learner birds. Nd, dorsal nidopallium.

Materials and Methods

Animals

All experiments using animals were performed according to the Hokkaido University Committee on Animal Experiments from whom permission of this study was obtained (Approval No. 13-0061). The guidelines follow the Japanese national regulations for animal welfare (Law for the Humane Treatment and Management of Animals; after the Partial Amendment No. 105, 2011). Animal surgery was performed under general anesthetics and animals were humanely killed by fast decapitation after being injected with a lethal dose of pentobarbital. Male zebra finches were obtained from Wada laboratory's breeding colony at Hokkaido University. The photoperiod was constantly maintained at a 13/11 h light/dark cycle with food and water provided *ad libitum*. The sex of the birds was checked by PCR to select male juveniles before experimental manipulation. Birds for the song developmental study were raised in individual breeding cages with their parents and siblings until phd 5–15. Juveniles (along with their siblings) were then raised in a sound-attenuation box by their mother with their siblings after removal of their father until they could feed themselves (phd ~35). Fathers were removed from the cages before phd 15, to ensure that the juveniles only heard the playback tutor from the start of the sensory learning phase. Juvenile birds were subsequently separated from their mother and siblings and housed in individual isolation boxes for song playback, with the same tutor song being played back from phd 30 to all developing juveniles until at least phd 140. Birds for the adult ablation experiments were raised in individual breeding cages with their parents and siblings

until phd 60–100 and then housed in common cages with other male birds. Control injected birds were used as controls in the $HVC_{(X)}$ ablation at the juvenile stage experiment instead of intact animals. This was possible because of the high stereotypy of song in zebra finches and also because comparison of control-injected birds to normal intact birds confirmed that control-injected birds were representative of the average intact juvenile. The total number of subject animals used was 42. 25 animals were used for the adult experiments, while 17 animals were used for the juvenile experiment.

Song recording, tutoring, and analysis

Songs were recorded using a unidirectional microphone (SM57, Shure, IL) connected to a computer with the sound event triggered by recording software Sound Analysis Pro (sap v2011.089; http://soundanalysispro.com/) (Tchernichovski et al., 2000). Each song bout was saved as a sound file (.wav file), including time information. Low frequency noise (< 0.5 kHz) and mechanical noise were filtered out using Avisoft-SASLab's (Avisoft Bioacoustics, Glienicke, Germany) band pass filter. With respect to song tutoring, birds were individually housed in a sound-attenuating box containing a mirror to reduce social isolation. Tutor songs were played five times in the morning and five times in the afternoon at 55–75 dB from a speaker (SRS-M30, SONY) passively controlled by Sound Analysis Pro.

For the analysis of similarity between pupil and tutor songs, the comparison of tutor and pupil syllable acoustic features was performed using the Sound Analysis Pro program's similarity module. The score was calculated using the "symmetric" and "time courses" comparison settings after manually adjusting the thresholds for every syllable. Overall, 80–

120 syllables, including multiple syllable types, were compared with syllables from tutor songs to obtain each similarity score between syllables in the pupil and tutor songs. The mean values of the similarity score for each syllable type in pupil songs against each syllable type in tutor songs were calculated, and the highest mean values were used as the similarity scores of each syllable type. We used the total mean value of the similarity scores of all syllable types for each individual bird. For the coefficient of variation (CV) of syllable similarity, the CV using the similarity scores of each syllable type was calculated for individual birds. To identify the new syllables appearing in pupil songs but not found in the tutor song, criteria of syllable duration and spectral similarity were used.

To analyze the syllable transitions, song similarity matrix (SSM) analysis was performed (Imai et al., 2016). For every bird and time point, 250 syllables from songs chosen randomly at phd 150 were used. Introductory notes in a song were not included in the song rendition. A total of 100 serially separated ".son"-converted syllable files were transferred to the Avisoft CORRELATOR program to calculate the similarity scores between the syllables of two songs by the round-robin comparison. The score was calculated as the peak correlation coefficient between two syllables according to the following formula:

$$\Phi_{XY} = \frac{\sum_X \sum_Y ((a_{xy} - m_a) * (b_{xy} - m_b))}{\sqrt{\sum_X \sum_Y (a_{xy} - m_a)^2 * \sum_X \sum_Y (b_{xy} - m_b)^2}}$$

where m_a and m_b are the mean values of the spectrograms a and b, respectively. a_{xy} and b_{xy} are the intensities of the spectrogram points at the locations x and y, respectively. The syllable similarity score is a value ranging from 0 to 1 for each syllable pair. In this study, 10 SSMs per bird were prepared by the round-robin comparison of a set of 50 serial syllables against another set of 50 syllables from the total of 250 syllables. To qualitatively

visualize the information of syllable temporal sequences in songs, each cell in the SSM was color coded according to the value of the similarity score. (**Figure M-1**) For the quantitative analysis of syllable temporal structures, the occurrence rate of characteristic patterns of binarized "2 row × 2 column" cells in the SSMs was calculated using the R software program. The "motif" pattern was defined as a "paired-syllables transition," indicating the existence of two successive syllables that were different but with the same sequential order in two songs. This can be illustrated by "song 1 [··A B·····] vs. song 2 [····A B····]" (in this case, A and B represent two different syllables). The "repeat" pattern was a case of the existence of the "repetitive-syllable transition" by two successive identical or very similar syllables in two songs: for instance, "song 1 [·····A A··] vs. song 2 [···A A·····]." The mean of the occurrence rate of the motif and repetition patterns and their coefficients of variation (CV) from 10 total SSMs per an individual animal were used for statistical analyses.

For song sequence analysis, song consistency was measured (Scharff and Nottebohm, 1991). Sequence consistency is calculated as the sum of typical transitions per bout divided by the sum of total transitions per bout. This measures how consistently the bird sings the same transitions over several bouts. Syllable identification was performed and aligned by two different researchers without information on individual birds. For highly variable syllables, identical syllables were characterized on the basis of acoustic morphology on the spectrogram and sequential position between singing renditions.

To measure the dynamics of syllable acoustic changes between two time points, we quantified changes in syllable acoustic features (mean FM, denoted as n) and syllable duration (ms; denoted as m) as two-dimensional scatter density plots. Kullback–Leibler

(K–L) divergence (Wu et al., 2008; Ohgushi et al., 2015), was adopted to measure the divergence between two sets of syllable populations by comparing their probability density distributions. Syllable segmentation was performed manually for all syllables on a SASLab spectrogram after increasing the amplitude intensity to the maximum in order to clarify any continuities/discontinuities in syllable boundaries. For every subject and time point, 150 syllables were used to generate a two-dimensional density scatter plot. The probability density functions of each set of syllables were estimated at two different time points a and b, as Qa and Qb for the two time points, and the K–L divergence score was then calculated to compare the density functions. If we let qa(m, n) and qb(m, n) denote the estimated probabilities for bin (20 bins for *m* and 5 bins for *n*) for time points a and b, respectively, then the K–L divergence between Qa and Qb is defined as follows:

$$DKL(Qa||Qb) = \sum_{m=a}^{M} \sum_{n=a}^{N} qa(m,n) \log_2 \frac{qa(m,n)}{qb(m,n)}$$

A larger value for K–L divergence corresponds to a lower similarity between the distributions of two sets of syllable populations at different time points. Thus, a K–L divergence of 0 indicates a perfect match between two sets of syllable populations. These behavioral analyses were performed as blind, without information of the residual number of $HVC_{(X)}$ neurons of each individual.

$HVC_{(X)}$ lesion effects on the variability of song acoustic structure was calculated by the two measures, “within-syllable variability” and “cross-rendition variability” of the fundamental frequency (FF) in song syllables (Kojima et al., 2018). 50 song motifs recorded on the pre-lesion day and those recorded on the post-lesion day were randomly

selected, extracting only the syllables that had clear and flat harmonic structure. For each syllable rendition, the trajectory of the fundamental frequency was obtained in a sound segment of harmonic structure as in a previous study (Charlesworth et al., 2012). Briefly, spectrograms were calculated using a Gaussian-windowed short-time Fourier transform (σ = 1 ms) sampled at 8 kHz, and the FF trajectory (the 1st harmonic frequency) was obtained by calculating the peak fundamental frequency in individual time bins. For a subset of syllables that exhibits relatively low signal-to-noise ratios in the 1st harmonic frequency, the 2nd or upper harmonic frequency was used to quantify the FF trajectory. For each syllable, FF trajectories of all renditions were aligned by the onset of the syllables, based on amplitude-threshold crossings, and flat portions ($\geq$ 25 ms) of FF trajectories were used for further analysis. We first removed the deviation of FF trajectories that was consistent across renditions of the same syllable by calculating residual FF trajectories as percent deviation from the mean trajectory across renditions. We then obtained within-syllable variability by calculating the SD of FF within each FF trajectory and averaging it across all renditions. To obtain cross-rendition variability, mean FF in each FF trajectory was calculated, and then the SD of mean FF across all renditions was computed.

In situ hybridization

NTS cDNA fragments used for the synthesis of *in situ* hybridization probes were cloned from a whole-brain cDNA mixture of a male zebra finch. Total RNA was transcribed to cDNA using Superscript Reverse Transcriptase (Invitrogen) with oligo dT primers. The cDNAs were amplified by PCR using oligo DNA primers directed to conserved regions

of the coding sequence from the NCBI cDNA database (accession # NM_001245684). PCR products were ligated into the pGEM-T Easy plasmid (Promega). The cloned sequences were searched using NCBI BLAST/BLASTX to compare with homologous genes with other species, and genome loci were identified using BLAT of the UCSC Genome Browser. For fluorescence *in situ* hybridization (FISH), digoxigenin (DIG)-labeled riboprobes were used. A total of 100–200 ng/glass of the DIG-labeled riboprobe was mixed with the hybridization solution [50% formamide, 10% dextran, 1× Denhardt's solution, 1 mM EDTA (pH 8.0), 33 mM Tris-HCl (pH 8.0), 600 mM NaCl, 0.2 mg/mL yeast tRNA, 80 mM dithiothreitol, and 0.1% N-lauroylsarcosine]. Hybridization was performed at 65 °C for 12–14 h. Washing steps were performed as follows: 5× SSC solution at 65 °C for 30 min, formamide-I solution (4× SSC, 50% formamide, and 0.005% Tween20) at 65 °C for 40 min, formamide-II solution (2× SSC, 50% formamide, and 0.005% Tween20) at 65 °C for 40 min, 0.1× SSC at 65 °C for 15 min × 2, 0.1× SSC at RT for 15min, NTE buffer at RT for 20 min, and TNT buffer × 3, and blocking buffer [1% DIG blocking solution (Roche) + 1% normal goat serum/1× TNT buffer] at RT for 30 min. DIG-labeled probes were detected with anti-DIG HRP-conjugated antibody (Jackson Laboratory) and a TSA Plus Cy5 system (Perkin Elmer). Signal images were obtained by fluorescence microscopy (EVOS FL; Thermo Fisher Science; BZ-X700; KEYENCE).

The number of $HVC_{(X)}$ neurons was estimated as the average NTS+ cells/mm^2 in both hemispheres of individuals. Based on the value of NTS+ cells/mm^2, the degree of ablation of $HVC_{(X)}$ neurons in individual birds was calculated as a normalized value (%) with the average of NTS+ cells/mm^2 of control birds.

Genetic switch mechanism for cell-specific targeting

In order to investigate the contribution of $HVC_{(X)}$ neurons to song learning and maintenance, a suitable method to manipulate this neuron population in behaving songbirds was needed. In rodents, straightforward methods for cell-specific manipulation are available, where genetically defined neuron types can be targeted using transgenic animals. While not available for all neuron types, this allows robust and simple targeting, using experimental procedures like mating transgenic mice from two strains with one another. In such a strategy, called a Cre/Lox system, one strain expresses an activating DNA recombinase protein, Cre, under a neuron type-specific promoter. The other strain carries an inverted Lox site-flanked DNA sequence (usually a flip-excision (FLEx) switch) encoding an effector protein that can only be expressed after DNA recombination by the Cre protein (Orban et al., 1992; Bouabe and Okkenhaug, 2013). Ideally, this translates into an intersectional targeting paradigm where the offspring expresses both transgenes, Cre and FLEx-encoded effector, only in the cell type determined by the promoter driving Cre expression (Branda and Dymecki, 2004; Madisen et al., 2015) (**Figure M-2*A***). New technical developments have increased the number of accessible cell types but have drawbacks, these techniques generally do not allow the investigation of specific pathways as they target whole cortical layers or interneuron populations (Gong et al., 2007; Taniguchi et al., 2011; Huang and Zeng, 2013). The lack of cell-type specificity was partially solved in mice by

surgically injecting viral vectors carrying the FLEx-encoded effectors into specific brain regions of mice expressing Cre in broad cell types (Rothermel et al., 2013; Rock et al., 2016; Tervo et al., 2016). The viral vector approach possesses other crucial advantages for the study of specific cell types, as some viral vectors like adeno-associated viruses (AAV) can move back from the injection area into upstream projection neurons by entering their axon terminals and riding back into the soma (Kaspar et al., 2002; Ahmed et al., 2004). The AAV retrograde capacity allows cell-specific targeting of specific projection neurons. Cell-specificity is reached by having a member of the pair -either Cre or FLEx- expressed in the projection neurons' somata and injecting the other member of the pair by way of a retrograding vector into the target region of the projection neurons (**Figure M-2*B***). In this way, if the experimenter avoids targeting reciprocally connected areas with retrograding vectors, the FLEx-encoded transgene is only expressed in the projection cell type of interest.

However, as useful as these techniques are in rodent models, they cannot be directly used in songbirds as the production of transgenic songbirds requires germ line manipulation via viral injection in fertilized eggs (Agate et al., 2009; Abe at al., 2015). Germline manipulation in songbirds is still an extremely costly and technically difficult process. To overcome this difficulty, in this study both Cre and the FLEx-encoded transgenes were expressed through adeno-associated virus injection into the brain regions of interest. As gene expression mediated by viral injection is potentially lower than the one provided by germline transgenes, a mutated form of the adeno-associated virus genome, the self-complementary adeno-associated virus (scAAV), was used to express the Cre and toxin proteins. Unlike single-stranded wild-type viruses, scAAV-containing particles carry double-stranded DNA. This double-stranded configuration

skips a crucial step in the AAV replication cycle and both speeds up and increases transgene expression in vivo (McCarty et al., 2001). In addition to using scAAVs, a combination of two cell-killing toxins were encoded each one inside the FLEx switches. These two toxins, diphtheria toxin A (dtA) and constitutively active Caspase 3 (caCasp) not only induce cell death, but also interact with each other, promoting their apoptotic effects (Komatsu et al., 1998; Kageyama et al., 2002). As previously found in Wada laboratory, a specific AAV capsid serotype, AAV9, allows retrograde transport and infection of projection neurons by AAV particles injected in these projection neurons' target areas.

To test the *in vivo* specificity of the Cre-FLEx system targeting of the $HVC_{(X)}$ neuron population, a vector containing a FLEx switch containing the reversed sequence of a red fluorescent protein (mRuby2), and a Cre-containing vector were co-injected in the adult zebra finch brain. In order to target the $HVC_{(X)}$ neuron population, an AAV9 vector encoding Cre (scAAV9-Cre) was injected into Area X while another AAV9 vector encoding FLEx-mRuby2 (scAAV9-mRuby2) was injected into HVC. As HVC projects to Area X through $HVC_{(X)}$ neurons but no neuron type within Area X is known to project back into HVC, fluorescent signal was expected to be found only in the $HVC_{(X)}$ neuron population. Additionally, in order to examine the time course of transgene expression, the same scAAV9-FLEx-mRuby2 and scAAV9-Cre viral combination was injected into the HVC and Area X of adult zebra finches that were then sacrificed at varying time points, from one week to 3 weeks after injection.

Adeno-associated virus (AAV) construction

All the viral ITR-flanked genomes used in this study were of the self-complementary (sc) AAV vector type (McCarty et al., 2001). The pscAAV-GFP vector containing a CMV promoter was obtained from Addgene (#32396). AAV plasmids containing Cre and DIO (double-floxed inverted open reading frame)/FLEx (Flip excision) inserts were obtained from Dr. Kenta Kobayashi from the National Institute of Physiological Sciences and subsequently cloned into the pscAAV vector plasmids after amplification of the Cre and DIO/FLEx sequences by primers containing the corresponding restriction enzymes in the target plasmid. To cell-specifically ablate the $HVC_{(X)}$ cells, a combination of diphtheria toxin A (dtA) and constitutively active caspase 3 was used (Lin et al., 1995; Foster et al., 2015; Walters et al., 2009).. Diphtheria toxin was cloned from pAAV-mCherry-FLEx-dtA (Addgene, #58536) by primers with specific enzyme sites and inserted into the previously constructed scAAV-DIO/FLEx. Owing to the restricted carrying capacity of the pscAAV vector, it became necessary to generate a constitutively active caspase 3 by insertional mutagenesis of rAAV-flex-taCasp3-Tevp obtained from Gene Therapy Center Vector Core at the University of North Carolina at Chapel Hill. This insertion consisted of the substitution of valine with glutamic acid at residue 266 of the protein, with subsequent amplification and cloning into an scAAV-DIO/FLEx vector.

AAVs were produced in-house using AAVpro 293T (Takara) cells transfected with a polyethyleneimine (PEI)-condensed recombinant DNA mixture, based on a protocol kindly provided to us by the Gradinaru Lab at Caltech. AAVpro 293T cells were amplified in 10 cm sterile culture dishes under standard cell culture medium [D-MEM, 10% fetal bovine serum (FBS), 1% penicillin, 1% GlutaMAX] until at least 1.5×10^8 cells could be collected. Cells were then plated onto 15 plates of 15 cm culture dishes at

1.0×10^7 cells per plate in standard cell culture medium. The confluence of the 15cm plates was checked visually, and the medium was changed again to standard 10% FBS medium when the confluence reached 80%, before proceeding to the transfection step. The transfection mix contained a triple plasmid system (pPack2/9 for serotype 2 Rep and serotype 9 Cap genes, pHelper for the adenoviral helper genes and the ITR-flanked viral genome containing plasmid) mixed with 40 kDa PEI in a 1: 3.5 DNA: PEI weight ratio, all dissolved in warm PBS. The cells were maintained in this transfection mix for 24 h, and then the medium was changed to a low serum one (D-MEM, 5% FBS, 1% penicillin, 1% GlutaMAX) to promote protein synthesis instead of cell division. Cells were scraped and collected in buffer (150 mM NaCl, 100 mM Tris-HCl pH 8.0) 3 days after transfection and maintained in a –80 °C freezer until viral purification. The purification procedure was performed as follows. Cells were freeze-thawed between a 37 °C water bath and a –80 °C cooled ethanol bath for at least four cycles and then incubated for 30 min in Benzonase (Merck-Millipore) nuclease after adding of 60 µL of 1 M $MgCl_2$ to the cell solution. At the end of this incubation, the cell solution was centrifuged at 4°C and 7,000 rpm for 1 h at 4°C, and then its supernatant was added as the top layer of a polycarbonate centrifuge column filled with an iodixanol gradient (15%, 25%, 40%, and 54% iodixanol layers). After ultracentrifugation for 6 h at 28,000 rpm, the 40% layer was extracted with a syringe and concentrated in four VivaSpin (Sartorius) cycles. Samples were finally aliquoted and stored in PBSF at –80 °C.

Surgery

Virus injection surgeries were performed on a custom-modified stereotaxic apparatus under 0.6–2.0% isoflurane anesthesia. To locate HVC and Area X, both stereotaxic coordinates from the midsagittal sinus "y point" (0 mm rostral–caudal and 2.0–2.2 mm medial–lateral from the y point for HVC, 7.8 mm rostral–caudal and 1.5 mm medial–lateral from the y point for Area X). Electrophysiological measurements using 1 M NaCl backfilled glass capillaries attached to a recording-capable Nanoject II (Drummond) were performed to locate HVC and Area X by visual inspection of the firing patterns of the target areas. The location of injection sites for juvenile birds was slightly different (roughly 0.3 mm shallower for Area X and closer to the midsagittal sinus for HVC), and special care was taken to shorten the surgery time as much as possible. The viral solution (virus titer 5.0×10^{12} to 5.1×10^{13} Vg/mL, a total of 1 μL in each Area X, and 800 nL in each HVC) was injected with a pressure Nanoject II.

Fluorescent tracers were injected into projecting areas to clarify whether NTS is expressed mainly in $HVC_{(X)}$ neurons instead of the other major projection neuron population in HVC, the $HVC_{(RA)}$ neuron population. The injected tracer was Cholera Toxin B (CTB) fused with the fluorochrome Alexa 555 or Alexa 465, injected into either Area X or nucleus RA. The sectioned slides from both injection treatments were hybridized against a DIG-labeled Neurotensin riboprobe to visualize Neurotensin mRNA localization.

Statistics

To account for the small sample size used, non-parametric tests were performed to determine the significance of the experimental results. Wilcoxon's rank-sum test was

used when comparing between two different non-normalized samples and Kendall's non-parametric test to probe for correlation between two variables from the same population. As an exception to the non-parametric tests, a one-sample t test was used after confirming normality to compare whether a normalized sample was statistically different from the reference value. Dunnett's test was used for pairwise comparisons between groups. All tests were performed by using the R statistical software.

Figure M-1

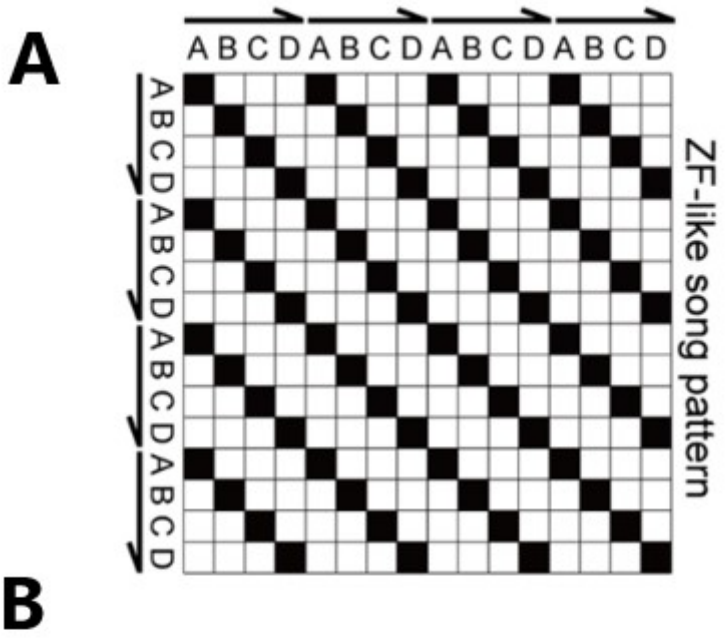

Syllable transition type		Syllable transitions meaning
Motif	A B / A B	Song1 (.....AB....) vs. Song2 (....AB.....)
Repeat	A A / A A	Song1 (.....AA....) vs. Song2 (....AA.....)

(A) Schematic diagram showing the method behind the Syllable Similarity Matrix (SSM) procedure to extract song patterns. Serial syllables of a bird's song are compared in a matrix against another set of serial syllables of the same bird and their spectrogram cross-correlation computed for all comparisons. Color shows a higher cross-correlation value, indicating higher similarity.

(B) Syllable transitions extracted based on the cross-correlation patterns displayed by the SSM matrix.

Figure M-2

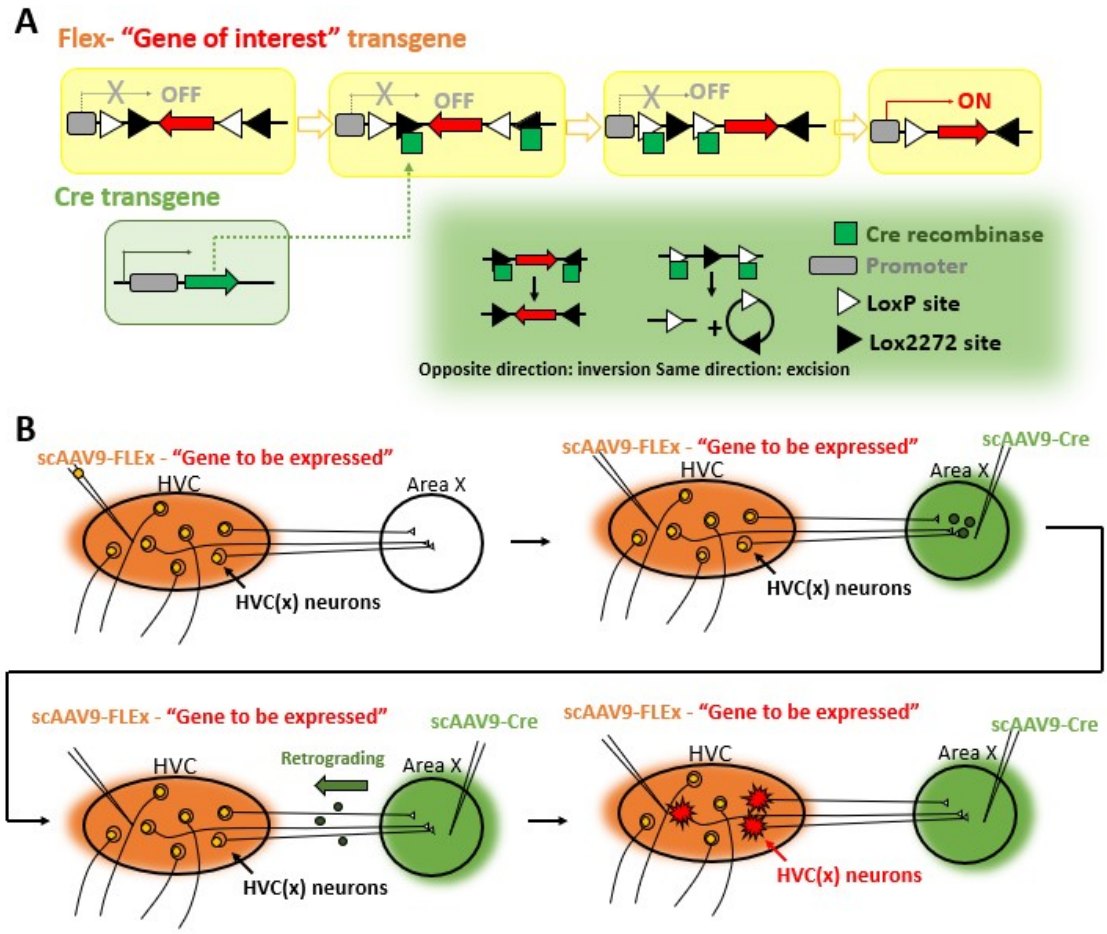
A
Flex- "Gene of interest" transgene
OFF
OFF
OFF
ON
Cre transgene
Cre recombinase
Promoter
LoxP site
Lox2272 site
Opposite direction: inversion Same direction: excision
B
scAAV9-FLEx - "Gene to be expressed"
HVC
Area X
HVC(x) neurons
scAAV9-FLEx - "Gene to be expressed"
HVC
Area X
scAAV9-Cre
HVC(x) neurons
scAAV9-FLEx - "Gene to be expressed"
scAAV9-Cre
HVC
Retrograding
Area X
HVC(x) neurons
scAAV9-FLEx - "Gene to be expressed"
scAAV9-Cre
HVC
Area X
HVC(x) neurons

A) Mechanism of functioning of the Cre-FLEx switch. Both transgenes are expressed in different constructs. When the Cre protein binds to any of its cognate sites (LoxP in white or Lox2272 in black), it either inverts or excises the DNA sequences between Lox sites depending on their orientation (green inset). This ensures that the inverted genes within the FLEx sequence will only be activated when Cre is expressed in the same cell.

B) Viral injection strategy for the expression of FLEx-flanked transgenes specifically in $HVC_{(X)}$ neurons. Small circles represent the scAAV9 viral particles.

Results

Successful cell-specific targeting of $HVC_{(X)}$ projection neurons

In order to test whether the Cre-FLEx switch system specifically targets $HVC_{(X)}$ neurons *in vivo*, adult bids were injected with scAAV9-Cre in Area X and scAAV9-FLEx-mRuby2 in HVC. Twenty days after viral injection, fluorescent label from mRuby2 was detected in a particular neuron population restricted to the boundaries of HVC (**Figure R-1*A***). No specific fluorescent signal arising from any other brain region could be detected. In the time course injected birds, clear mRuby2 fluorescent signal could be detected from the first week after injection onwards (**Figure R-1*B***). In summary, the combined Cre-FLEx viral strategy allows for strong $HVC_{(X)}$ neuron-specific transgene expression from at least one week after injection *in vivo*.

Identification of Neurotensin as a specific $HVC_{(X)}$ neuron marker

To count the remaining amount of $HVC_{(X)}$ neurons after ablation, a reliable $HVC_{(X)}$-specific gene marker was needed. To attain this goal, the efficacy of neurotensin (NTS) as an $HVC_{(X)}$ maker was tested using sections from birds with $HVC_{(X)}$ or $HVC_{(RA)}$ populations labeled by the injection of retrograde CTB-555. (**FigureR-2*A***). NTS showed an above 95% colocalization with fluorescent tracer backfilled from Area X and an almost negligible colocalization with tracer coming from nucleus RA. The above result confirms NTS as an $HVC_{(X)}$ neuron-specific marker that can be used to precisely count the remaining $HVC_{(X)}$ cells without needing any additional fluorescent tracer injections before brain collection.

A majority of HVC$_{(X)}$ neurons were ablated by a combination of viral vectors encoding Cre recombinase and cell-killing toxins

To check whether HVC$_{(X)}$ neuron-specific activation of both dtA and caCasp is effective *in vivo*, adult zebra finches were injected in one hemisphere's HVC with a mix of scAAV9-FLEx-dtA and scAAV9-FLEx-caCasp to induce HVC$_{(X)}$ neuron ablation and scAAV9-FLeX-mRuby2 in the other hemisphere's HVC as a negative control (**Figure R-2*B***). The use of a control and an HVC$_{(X)}$ ablated hemisphere from the same individual birds avoids any potential between-individual differences in HVC$_{(X)}$ number or density. As a result, the residual number of HVC$_{(X)}$ neurons was reduced to 23.9–57.2% (mean ± SD = 38.8 ± 13.5%) in the ablated hemisphere when compared against the control HVC of the same individual (n = 6; One sample *t* test after confirmation of normality by Shapiro-Wilk test: $p < 0.001$). All groups of HVC$_{(X)}$ neuron-ablated birds used in the three experiments in this study showed HVC$_{(X)}$ ablations of over 70% when compared to controls (**Figure R-3**). Although no complete lesion (i.e., 100 % ablation) of the HVC$_{(X)}$ population in a single hemisphere was achieved, a major part of the population could be reliably ablated with the viral combination of Cre and cell-killing toxins.

HVC$_{(X)}$ neuron ablation during the critical period impairs song learning and development

To elucidate the contributions of the HVC$_{(X)}$ neurons to song learning, a combination of viruses was injected in the HVC and Area X (**Figure R-4*A***). In the case of HVC$_{(X)}$ neuron-ablated juveniles, retrograding scAAV9-Cre was injected into bilateral Area X,

while a mix of scAAV9-FLEx-dTA and scAAV9-FLEx-caCasp was injected into bilateral HVC. Control juveniles were injected with scAAV9-Cre in bilateral Area X and scAAV9-FLEx-mRuby2 in bilateral HVC. In both cases injections were performed before the start of subsong in young juveniles (20-30 phd). Juveniles were then tutored with the same tutor song by speaker playback throughout their song developmental period (tutoring lasted at least until 140 phd) (**Figure R-4*A***, top right). The degree of $HVC_{(X)}$ ablation in individual birds ranged from 68.6 to 76.3% (mean ± SD, 73.0 ± 2.8%) (**Figure R-3**).

$HVC_{(X)}$ neuron ablation at the juvenile stage caused multiple effects in the song acoustics and sequence of their adult songs when compared to the adult songs of control-injected juveniles (**Figure R-4*B***). Control-injected juveniles developed an acoustically similar song to their tutor, with a stereotyped motif sequence (**Figure R-5**, white bars) that crystallized around 120 phd, at the typical closure time of the song critical period (**Figure R-5**, top panel for a representative example). In contrast, two $HVC_{(X)}$-ablated juveniles developed a song acoustically dissimilar to their tutor during a more protracted developmental course (**Figure R-5**, bottom two panels). While the song of one $HVC_{(X)}$-ablated juvenile finally converged into a species-typical song motif (**Figure R-5**, middle panel), the other example bird never crystallized a song motif and kept singing songs with an ever-changing sequence until past 200 phd (**Figure R-5**, bottom panel). $HVC_{(X)}$ ablation never impeded the appearance of discrete song syllables or halted the transition from subsong to plastic song. However, earning of acoustic and sequence properties in their final adult songs and were affected in the $HVC_{(X)}$ neuron-

ablated birds at the juvenile stage. Additionally, the length of the critical period was affected in some birds.

$HVC_{(X)}$ neuron ablation during the critical period of song learning disrupts syllable acoustics

Focusing on the adult (150 phd) syllables sung by injected pupils, some $HVC_{(X)}$-ablated learned less syllables from the tutor song (Wilcoxon's signed rank test: $p = 0.048$) and developed new syllables never seen in the tutor songs (Wilcoxon's signed rank test: $p = 0.031$) (**Figure R-6*A***). Furthermore, the acoustic similarity between the $HVC_{(X)}$-ablated bird's own syllables and the tutor song's syllables was significantly lower than the similarity of control-injected pupils' syllables compared to the tutor (Wilcoxon's signed rank test: $p = 0.035$) (**Figure R-6*B,*** top). Additionally, the coefficient of variability (CV) of acoustic similarity to the tutor showed a trend towards increase in the $HVC_{(X)}$-ablated bird group (Wilcoxon's signed rank test: n.s., $p = 0.071$) (**Figure R-6*B,*** bottom). Thus, acoustic imitation of tutor song was affected both at the bulk level of the number of syllables learned from the tutor and at the finer level of acoustic similarity between individual syllables.

Still at the syllable level, two of five $HVC_{(X)}$-ablated birds ablated at the juvenile stage showed a remarkably high degree of acoustic and syllable length variability at the adult stage (over 120 phd). Selected examples of the same syllable taken from the afternoon song of a single day (150 phd) in one control-injected and two $HVC_{(X)}$ ablated birds show the ever-changing duration of specific syllables compared to those from a control bird (**Figure R-7*A***). Some birds (two out of five), also sang songs with very short inter-

syllable gaps (average of gap duration < 25 ms). While the control-injected songbird produced songs with gaps similar in length to the tutor song, two $HVC_{(X)}$-ablated pupils displayed markedly shortened gaps (**Figure R-7*B***). While there was a trend towards shortened inter-syllable gaps in some $HVC_{(X)}$-ablated pupils, no statistically significant difference was found between control and $HVC_{(X)}$-ablated groups due to the occurrence of individual difference (Wilcoxon's signed rank test: n.s., $p = 1$) (**Figure R-7*C***). In summary, some $HVC_{(X)}$-ablated pupils showed aberrant acoustics as well as variability in syllable length and/or shortened inter-syllable gaps well into adulthood.

Species-specific song pattern is severely affected by $HVC_{(X)}$ ablation during the critical period

The effects of $HVC_{(X)}$ neuron ablation on song sequence were analyzed by performing SSM analysis on the adult songs of $HVC_{(X)}$-ablated birds. Control-injected birds produced songs with motif patterns clearly visible in the matrix, while $HVC_{(X)}$-ablated birds produced songs with a range of lower motif values (**Figure R-8*A***). The $HVC_{(X)}$-ablated pupil group produced significantly less motif patterns when compared to the control-injected group pupils (n = 3 controls, n = 5 ablated birds; 250 syllables each) (Wilcoxon's signed rank test: $*p = 0.035$), while the apparent increase in repetition pattern did not reach significance **(Figure R-8*B***).

In order to analyze whether the effects of $HVC_{(X)}$ ablation on acoustics and sequence arise from common mechanisms or not, the correlation between acoustic similarity to tutor and SSM-derived motif index was analyzed for every individual **(Figure R-8*C***). No correlation between the effects of $HVC_{(X)}$ ablation on acoustics and its effects on

sequence was found (Kendall's tau: n.s., p = 0.179). Considering the above results, $HVC_{(X)}$ neuron ablation in zebra finch juveniles affects the learning and acquisition of tutor song acoustics and species-specific song motif patterns through unrelated mechanisms.

$HVC_{(X)}$ ablation at the adult stage does not disrupt song nor AFP-driven vocal fluctuation

In order to investigate the role of $HVC_{(X)}$ neurons, adult zebra finches (90-120 phd) singing clear motif patterns were injected with the same $HVC_{(X)}$-ablating viral mixture as the one used in the juvenile study. The $HVC_{(X)}$ ablation amount in the ablated adults ranged from 68.3 to 86.1% (mean ± SD, 79.1 ± 8.3%) (**Figure R-3**). Visual inspection of the songs produced afterwards showed no gross alterations in acoustics or sequence, either 2 weeks after or a few days after injection. The 3 to 4 days after injection time point was used as a control to check for any possible injection-related damage as viral transgenes are not expressed yet (**Figure R-9*A***). Quantification of remaining $HVC_{(X)}$ neurons by *in situ* hybridization against NTS confirmed the extent of ablation in adult $HVC_{(X)}$-ablated birds (**Figure R-9*B***). Despite this, no significant changes were seen after two weeks in $HVC_{(X)}$-ablated birds, either by SSM analysis or by plotting acoustic parameters against syllable duration (**Figure R-9*C***). Taking all $HVC_{(X)}$-ablated adult birds into account (n = 4), motif indices were left unchanged after $HVC_{(X)}$ ablation (Wilcoxon's signed rank test: n.s., p = 0.685) (**Figure R-9*D***). To evaluate any potential change in fine acoustics the K-L divergence method was used to compute the divergence between pairs of before and after $HVC_{(X)}$-ablation acoustic parameter plots

(using mean frequency modulation versus syllable duration) in injected birds and in age-matched control zebra finches. As expected from the visual inspection of song spectrograms and plotted acoustic parameters, acoustic K-L divergence between the control and $HVC_{(X)}$-ablated group was not different among groups (Wilcoxon's signed rank test: n.s., $p = 1$) (**Figure R-9*E***). Motif duration was additionally quantified in order to check for changes in song tempo after $HVC_{(X)}$ ablation, but no statistically significant differences between control and $HVC_{(X)}$-ablated groups were found either (Wilcoxon's signed rank test: n.s., $p = 0.857$) (**Figure R-9*F***).

As described in a previous study (Kojima et al., 2018), vocal fluctuation related to AFP output correlates best with within-syllable fundamental frequency (FF) variability than with cross-syllable FF variability. Accordingly, the effects of adult $HVC_{(X)}$ ablation on AFP output were tested by measuring the amount of vocal fluctuation after $HVC_{(X)}$ neuron ablation. The deviation from mean in FF was quantified from the syllables obtained from 50 song bouts produced both before and after $HVC_{(X)}$ ablation (**Figure R-10*A***). FF analysis found no effects of $HVC_{(X)}$ ablation both at the within-syllable (Wilcoxon's signed rank test: n.s., $p = 0.857$) and cross-syllable FF variability levels (Wilcoxon's signed rank test: n.s., $p = 1$) (**Figure R-10*B***).

Considering the adult zebra finch $HVC_{(X)}$ ablation results, no effects of $HVC_{(X)}$ ablation on adult song acoustics, sequence or bout duration could be found, nor was AFP output as measured by fluctuation in FF frequency at the within-syllable level affected by $HVC_{(X)}$ ablation.

$HVC_{(X)}$ ablation at the adult stage has no effects on auditory feedback-dependent song degradation

An additional way of measuring the amount of adult song plasticity is to probe the ability of birds to modify their songs after auditory feedback loss. In order to confirm any possible role of $HVC_{(X)}$ neurons in auditory feedback-dependent song degradation, surgical deafening was performed three weeks after injection of the $HVC_{(X)}$-ablating viral mix (**Figure R-11*A***). $HVC_{(X)}$ ablation ranged in the birds used for this experiment from 66.2 to 78.8% (mean ± SD, 72.2 ± 5.3%) (**Figure R-3**). The song degradation rate was then compared between the $HVC_{(X)}$-ablated and deafened birds and a group of deafened-only birds ($HVC_{(X)}$-ablated and deafened birds n = 5, deafened only controls n = 5). When measured at one and two months after deafening, song acoustics and sequence degraded in a similar way when compared to the original song pre-deafening (**Figure R-11*B***). Song sequence degradation in $HVC_{(X)}$-ablated deaf birds was strong for all animals (Wilcoxon's signed rank test between pre and 2 months after deafening: p = 0.00016), with $HVC_{(X)}$ ablated birds showing a similar level of song motif degradation compared to control deafened birds at two moths post-deafening (Wilcoxon's signed rank test: n.s., p = 0.841) (**Figure R-11*C***). Similarly, the level of song acoustic degradation as measured by K-L divergence from both control and $HVC_{(X)}$ ablated birds between pre and two months after deafening was strong (Wilcoxon's signed rank test between pre and 2 months after deafening: p = 0.00001). However, the difference in K-L divergence between $HVC_{(X)}$-ablated deaf birds and deaf controls at two months after deafening was both non-statistically significant and did not seem to be related to the remaining number of $HVC_{(X)}$ projection neurons (Wilcoxon's signed rank test: n.s., p = 1) (**Figure R-11*D***). In summary, $HVC_{(X)}$ ablation at the adult

stage has no effect on the AFP output as measured by FF fluctuation or measured by the magnitude of song degradation after removal of auditory feedback-dependent song maintenance.

Figure R-1

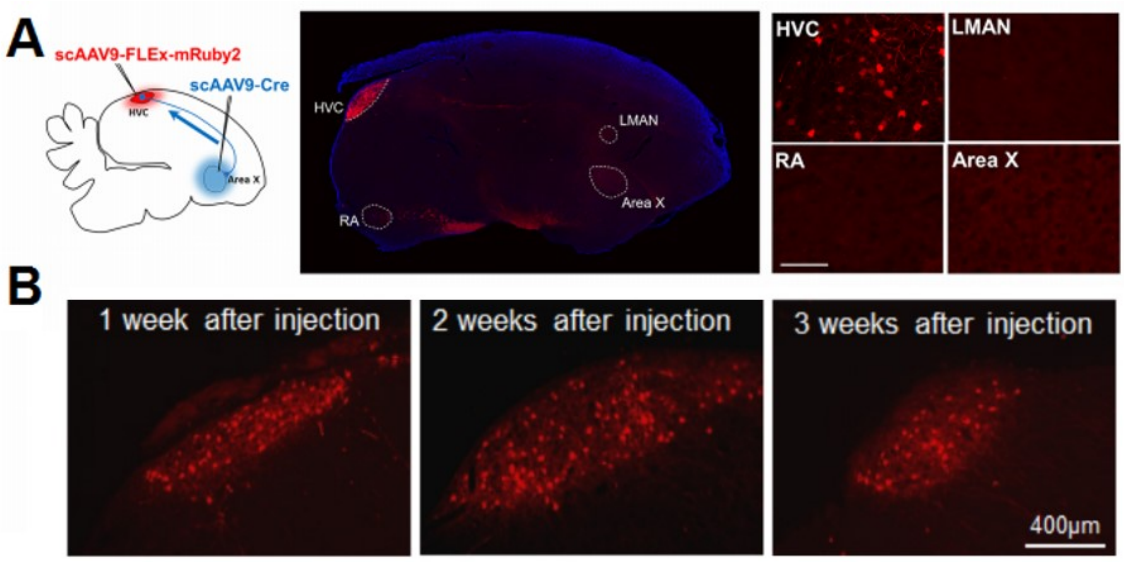
A
scAAV9-FLEx-mRuby2
scAAV9-Cre
HVC
Area X
HVC
LMAN
RA
Area X
HVC
LMAN
RA
Area X
B
1 week after injection
2 weeks after injection
3 weeks after injection
400μm

A) (Left diagram) $HVC_{(X)}$ projection neurons were targeted using a combination of retrograding scAAV9-Cre injected in basal ganglia nucleus Area X and scAAV9-FLEx-mRuby2 injected in HVC. (Right panels) Restricted expression of FLEx-inverted mRuby2 fluorescent protein in the $HVC_{(X)}$ cell population. Scale bar = 100mm.

B) Restricted expression of FLEx-inverted mRuby2 fluorescent protein in $HVC_{(X)}$ cell populations at 1, 2 and 3 weeks after virus injection. Apparent differences in HVC size between animals are due to the brain slices coming from different medial-lateral positions in nucleus HVC.

Figure R-2

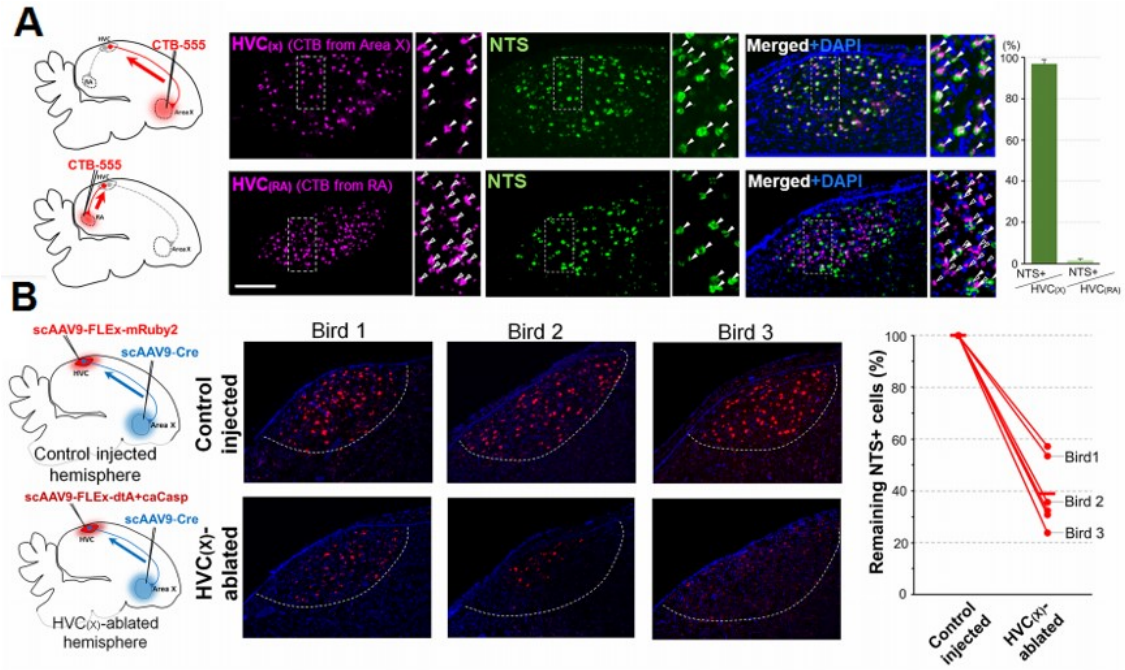
A
CTB-555
HVC(x) (CTB from Area X)
NTS
Merged+DAPI
CTB-555
HVC(RA) (CTB from RA)
NTS
Merged+DAPI
(%)
100
80
60
40
20
0
NTS+ HVC(x)
NTS+ HVC(RA)
B
scAAV9-FLEx-mRuby2
scAAV9-Cre
Control injected hemisphere
scAAV9-FLEx-dtA+caCasp
scAAV9-Cre
HVC(x)-ablated hemisphere
Bird 1
Bird 2
Bird 3
Control injected
HVC(x)-ablated
Remaining NTS+ cells (%)
100
80
60
40
20
0
Bird1
Bird 2
Bird 3
Control injected
HVC(x)-ablated

A) Selective expression of NTS in $HVC_{(X)}$ neurons (green fluorescence shows DIG-labeled NTS riboprobes detected by Cy5-conjugated antibodies). $HVC_{(X)}$ and $HVC_{(RA)}$ neurons were backfilled with the retrograde tracer CTB-555 from Area X and RA, respectively (magenta). DAPI (blue).

B) Normalized decreased amount of $HVC_{(X)}$ neurons between control (left) and lesioned HVC. The control hemisphere was injected with scAAV9-Cre in Area X and with scAAV9-FLEx-mRuby2 in HVC. The lesioned hemisphere was injected with scAAV9-Cre in Area X and with a mixture of scAAV9-FLEx-dtA and -caCasp in HVC.

Figure R-3

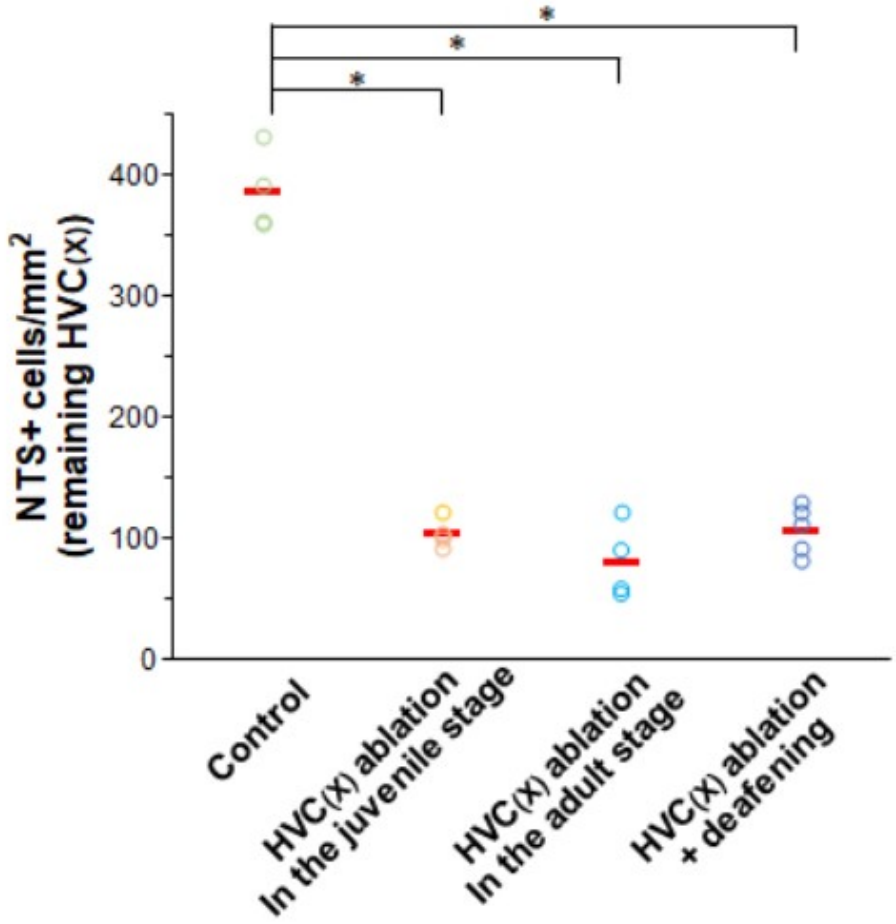
*
*
*
400
300
200
100
0
NTS+ cells/mm2
(remaining HVC(X))
Control
HVC(X) ablation
In the juvenile stage
HVC(X) ablation
In the adult stage
HVC(X) ablation
+ deafening

Comparison of remaining $HVC_{(X)}$ neurons among control, ablation in the juvenile stage, adult stage, and following deafening conditions. Each dot corresponds to the average density of NTS+ cells ($HVC_{(X)}$ neurons) in one bird. Red horizontal bars represent the mean values for each group (Dunnett's test, $*p = 0.017$).

Figure R-4

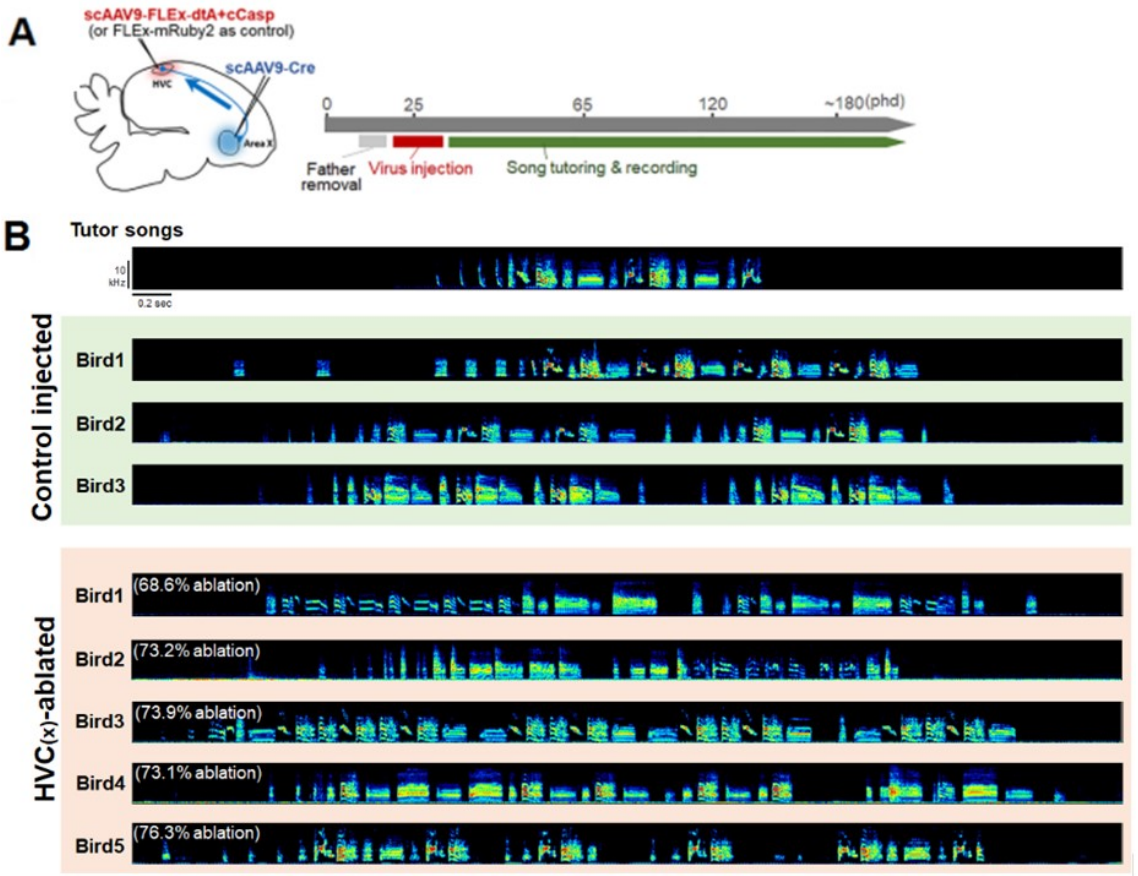
A
scAAV9-FLEx-dtA+cCasp
(or FLEx-mRuby2 as control)
scAAV9-Cre
HVC
Area X
0
25
65
120
~180(phd)
Father removal
Virus injection
Song tutoring & recording
B
Tutor songs
10 kHz
0.2 sec
Control injected
Bird1
Bird2
Bird3
HVC(x)-ablated
Bird1 (68.6% ablation)
Bird2 (73.2% ablation)
Bird3 (73.9% ablation)
Bird4 (73.1% ablation)
Bird5 (76.3% ablation)

(A) Experimental timeline for $HVC_{(X)}$ ablation and song tutoring.

(B) Examples of acquired song at 180 phd in all control-injected (green-colored background) and all $HVC_{(X)}$-ablated (brown-colored background) birds. Bird numbers are consistent between figures in the Results section.

Figure R-5

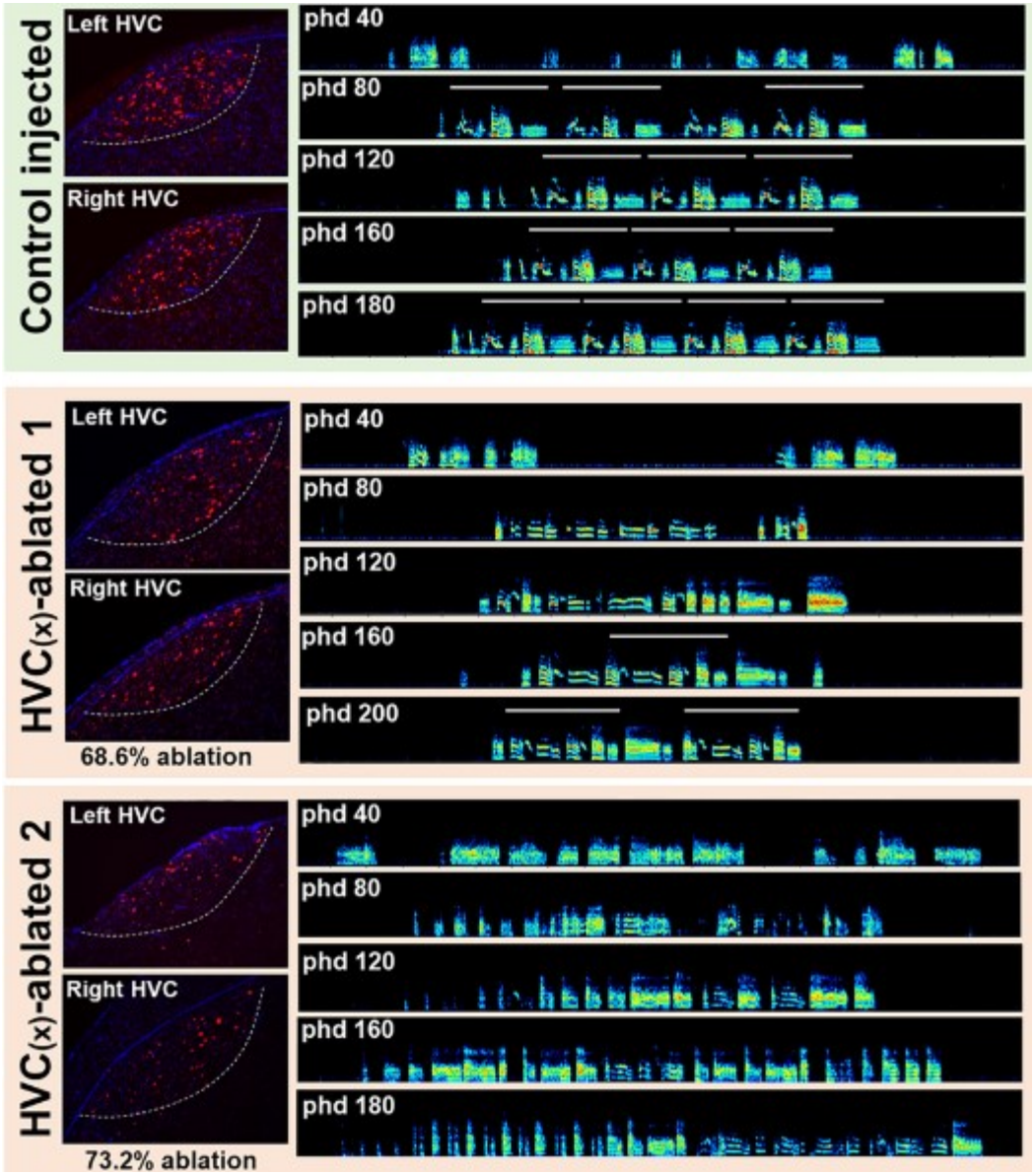
Control injected
Left HVC
Right HVC
phd 40
phd 80
phd 120
phd 160
phd 180
HVC(x)-ablated 1
Left HVC
Right HVC
68.6% ablation
phd 40
phd 80
phd 120
phd 160
phd 200
HVC(x)-ablated 2
Left HVC
Right HVC
73.2% ablation
phd 40
phd 80
phd 120
phd 160
phd 180

Examples of song development in a control injected (green-colored background) and two $HVC_{(X)}$-ablated (brown-colored background) birds. $HVC_{(X)}$-ablated birds 1 and 2 had decreases of 68.6 and 73.2% of $HVC_{(X)}$ neurons, respectively, compared with the average of $HVC_{(X)}$ neurons in the control birds. White lines in the song spectrograms represent the motif structure of songs. The remaining $HVC_{(X)}$ neurons were labeled with NTS (red). DAPI (blue). White dotted lines represent HVC borders.

Figure R-6

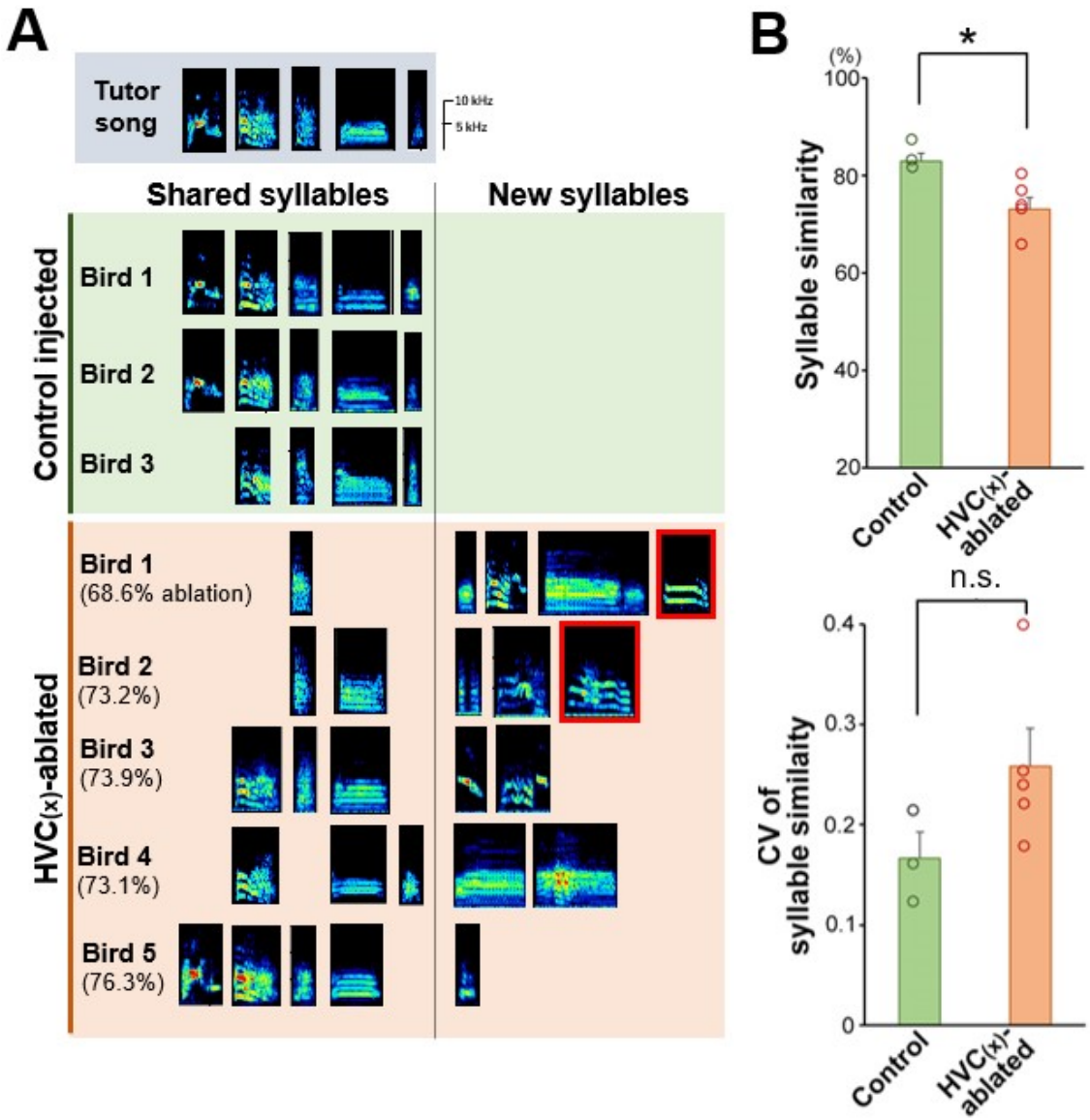
A
Tutor song
10 kHz
5 kHz
Shared syllables
New syllables
Control injected
Bird 1
Bird 2
Bird 3
HVC(x)-ablated
Bird 1
(68.6% ablation)
Bird 2
(73.2%)
Bird 3
(73.9%)
Bird 4
(73.1%)
Bird 5
(76.3%)
B
*
(%)
100
80
60
40
20
Syllable similarity
Control
HVC(x)-ablated
n.s.
0.4
0.3
0.2
0.1
0
CV of syllable similaity
Control
HVC(x)-ablated

(A) Examples of acquired syllables in control (green background) and $HVC_{(X)}$-ablated (brown-colored background) birds. Syllables outlined with red lines were further analyzed in **Figure R-7*A***.

(B) Differences between control and $HVC_{(X)}$-ablated birds in the syllable similarity between syllables of each pupil and the tutor song (left) and its CV (right) (n = 3 controls, n = 5 ablated birds; Wilcoxon's signed rank test: $*p = 0.035$). Mean + SEM for bar graphs. (Left) Each point represents the average similarity score of all syllable types for individual birds. (Right) Each point represents the CV of the similarity scores of all syllable types for individual birds.

Figure R-7

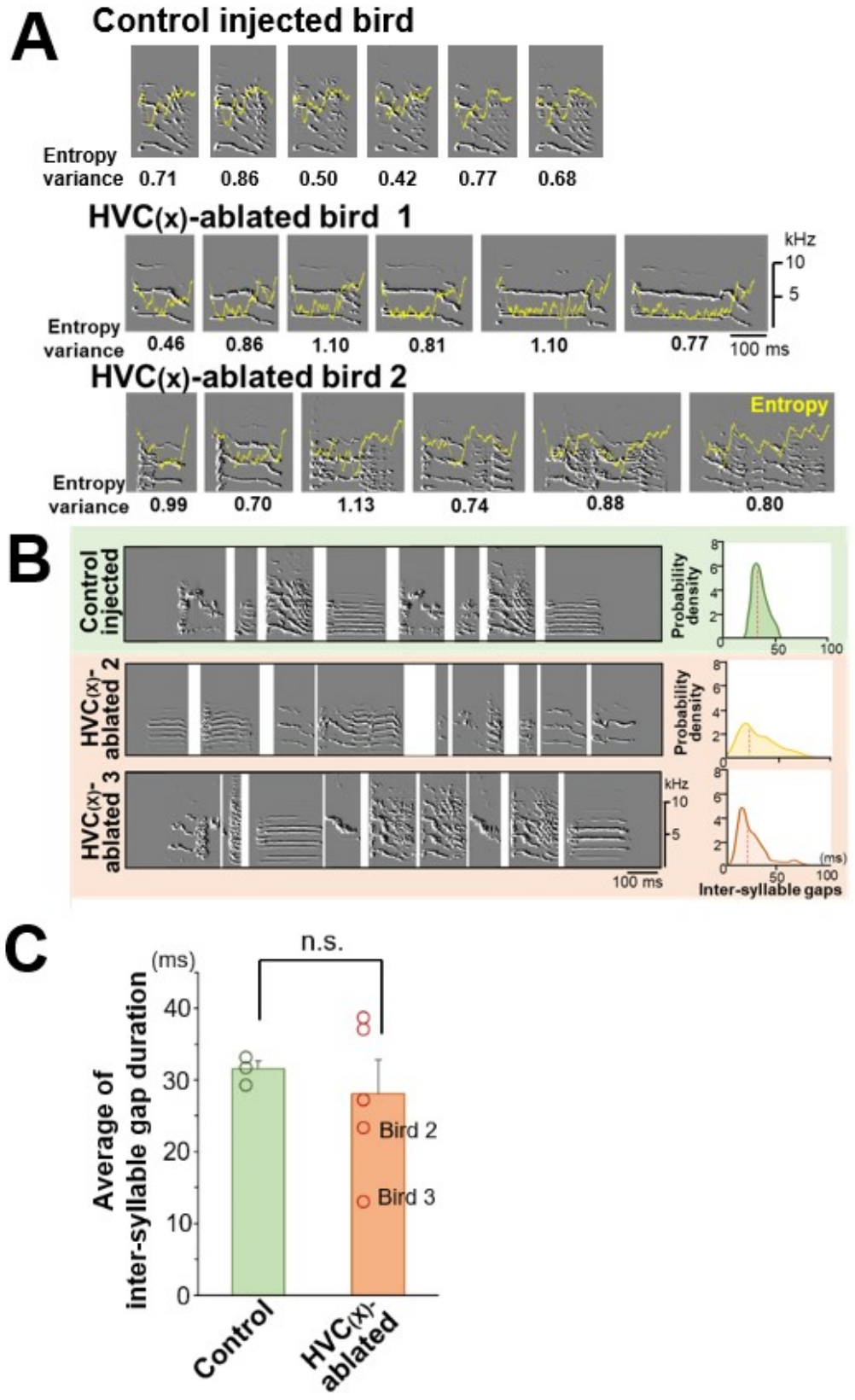
A
Control injected bird
Entropy variance
0.71
0.86
0.50
0.42
0.77
0.68
HVC(x)-ablated bird 1
kHz
10
5
Entropy variance
0.46
0.86
1.10
0.81
1.10
0.77
100 ms
HVC(x)-ablated bird 2
Entropy
Entropy variance
0.99
0.70
1.13
0.74
0.88
0.80
B
Control injected
HVC(x)-ablated 2
HVC(x)-ablated 3
Probability density
kHz
10
5
100 ms
(ms)
Inter-syllable gaps
C
n.s.
(ms)
Average of inter-syllable gap duration
40
30
20
10
0
Bird 2
Bird 3
Control
HVC(x)-ablated

(A) High variability in syllable duration and acoustics at the adult stage (150 phd) for birds whose $HVC_{(X)}$ neurons were ablated in the juvenile stage. Yellow lines represent acoustic entropy, and numerical values show entropy variance.

(B) Examples of abnormal inter-syllable gaps in the adult stage for birds whose $HVC_{(X)}$ neurons were ablated in the juvenile stage. (Left) Variability and shortening of inter-syllable gaps in $HVC_{(X)}$-ablated birds in the juvenile stage. (Right) Probability density of inter-syllable gaps from each bird (n = 100 gaps). The red dotted lines indicate average values.

(C) Average of inter-syllable gap duration between control and $HVC_{(X)}$-ablated birds (100 inter-syllable gaps/bird). There was no difference in gap duration between control and $HVC_{(X)}$ ablated birds (Wilcoxon's signed rank test: n.s., $p = 1$). Each dot represents an individual bird's value. Bird ID numbers are consistent between with **Figure R-7*A***.

Figure R-8

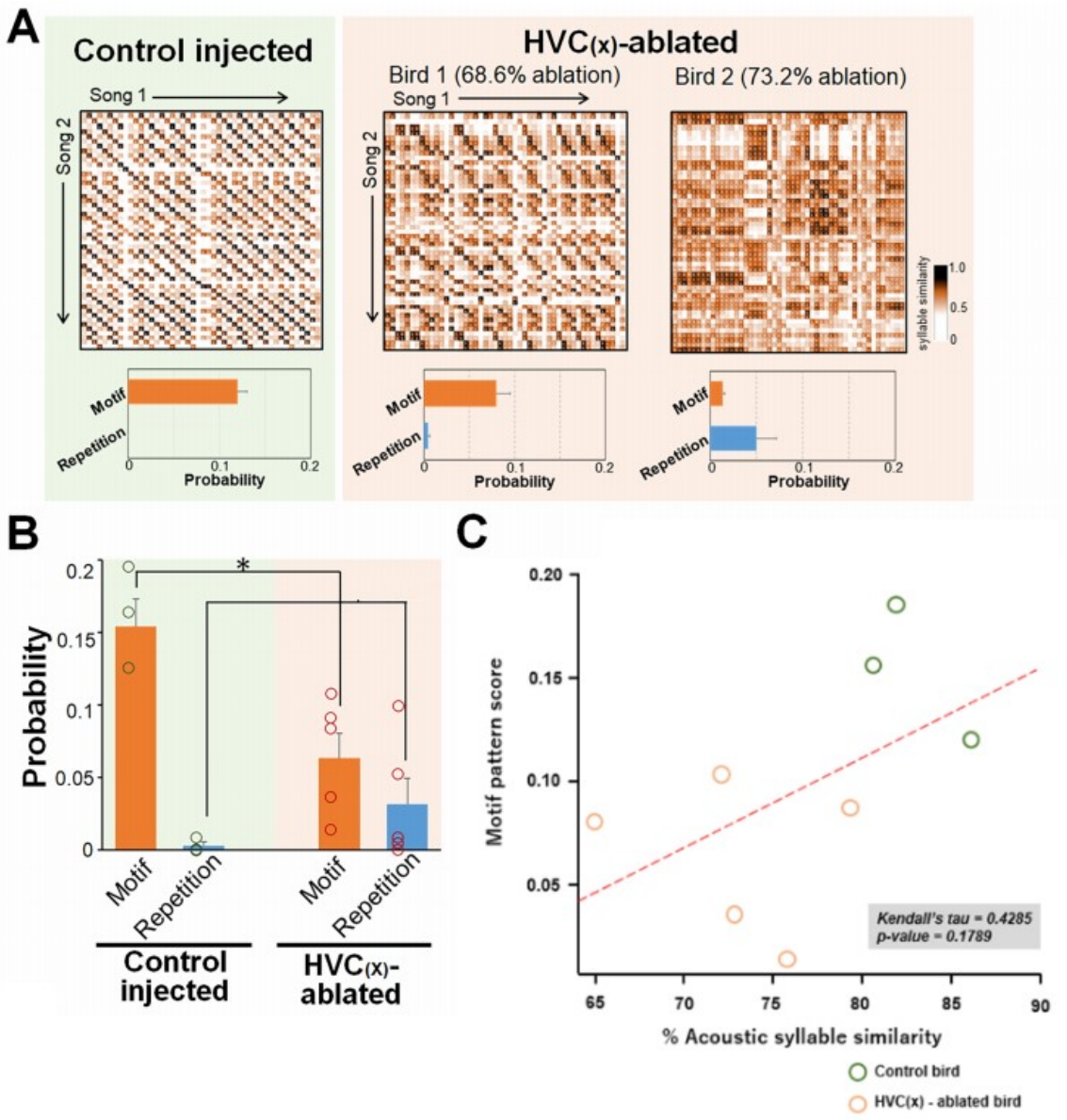
A
Control injected
Song 1
Song 2
Motif
Repetition
Probability
HVC(x)-ablated
Bird 1 (68.6% ablation)
Bird 2 (73.2% ablation)
syllable similarity
B
Probability
Control injected
HVC(x)-ablated
C
Motif pattern score
% Acoustic syllable similarity
Kendall's tau = 0.4285
p-value = 0.1789
Control bird
HVC(x) - ablated bird

(A) Representative syllable similarity matrices (SSMs) for adult songs (150 phd) in control (green background) and two $HVC_{(X)}$-ablated (brown background) birds. (Bottom) Probabilities of motif and repetition indices for each bird.

(B) Probabilities of motif and repetition indices in the adult stage (150 phd) in control and $HVC_{(X)}$-ablated birds (n = 3 controls, n = 5 ablated birds; Wilcoxon's signed rank test: $*p = 0.035$). Dots indicate individual bird's values.

(C) Lack of correlation between the SSM-derived motif scores and the acoustic similarity to tutor (n = 3 controls, n = 5 ablated birds; Kendall's tau: n.s., $p = 0.179$). Dots indicate individual bird's values.

Figure R-9

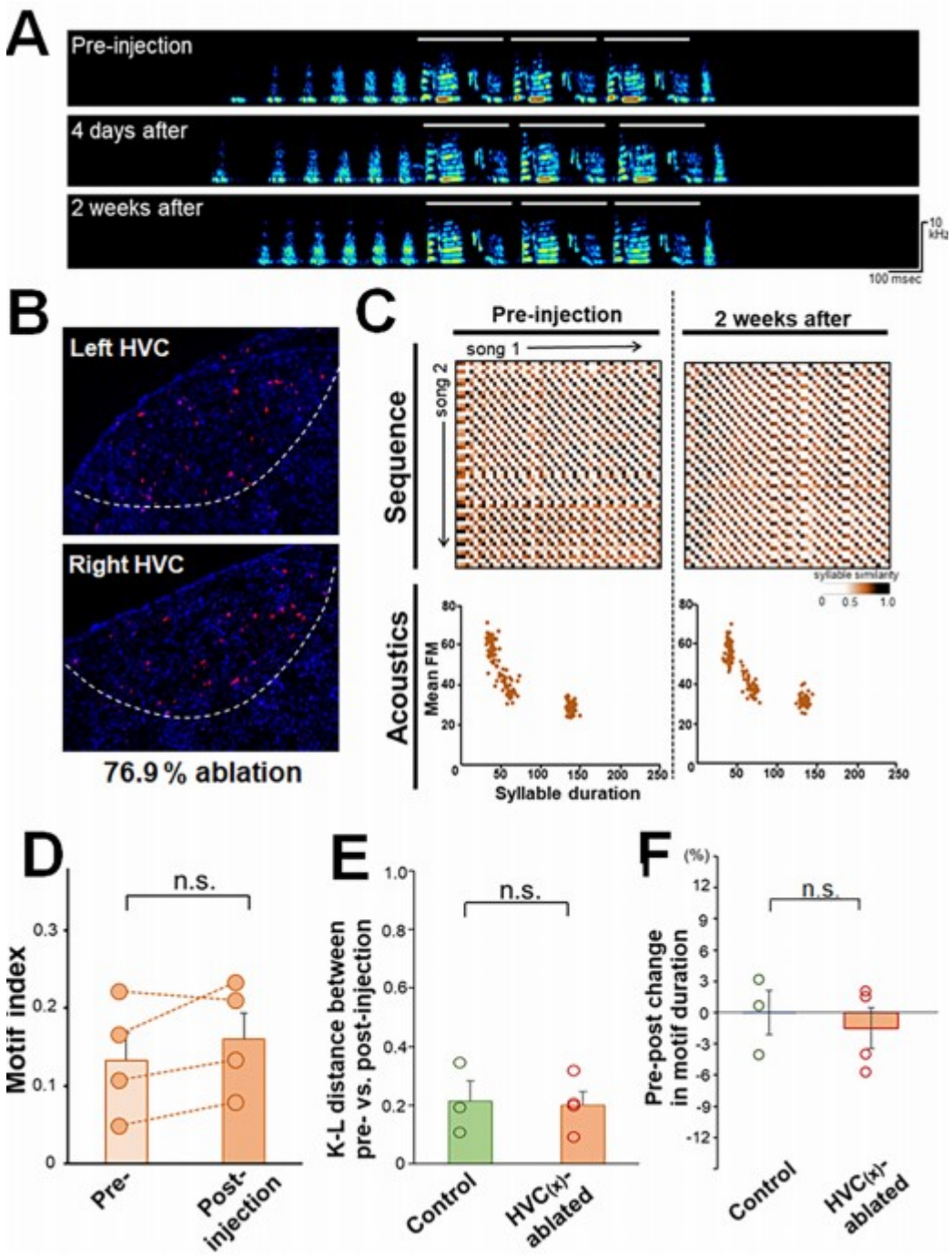
A
Pre-injection
4 days after
2 weeks after
10 kHz
100 msec
B
Left HVC
Right HVC
76.9 % ablation
C
Pre-injection
2 weeks after
song 1
song 2
Sequence
syllable similarity
0 0.5 1.0
Acoustics
Mean FM
Syllable duration
D
Motif index
n.s.
Pre-
Post-injection
E
K-L distance between pre- vs. post-injection
n.s.
Control
HVC(x)-ablated
F
Pre-post change in motif duration
(%)
n.s.
Control
HVC(x)-ablated

(A) Representative spectrogram of birds that were ablated in $HVC_{(X)}$ neurons in adults. White bars represent the motif structure of songs.

(B) Example of the extent of $HVC_{(X)}$ ablation in an ablated adult (with 76.9 % ablation) as shown in **(A)** and **(C)**. NTS (red) and DAPI (blue).

(C) Syllable sequence and acoustic stability before and after ablation of $HVC_{(X)}$ neurons. Sequential patterns are shown as SSMs and acoustics as a scatter density plot of syllable duration versus mean FM (n = 150 syllables).

(D) No effect of $HVC_{(X)}$ ablation on the song motif index of adult zebra finches. Each point corresponds to an individual bird. (n = 4 ablated birds; Wilcoxon's signed rank test: n.s., $p = 0.685$).

(E) No effect of $HVC_{(X)}$ ablation on syllable acoustics measured by the K-L divergence of syllable scatter density plots (duration versus mean FM) between pre- and post-injection time points (n = 3 controls, n = 4 ablated birds; Wilcoxon's signed rank test: n.s., $p = 1$).

(F) Pre–post change in motif duration between control and $HVC_{(X)}$-ablated birds (Wilcoxon's signed rank test: n.s., $p = 0.857$).

Figure R-10

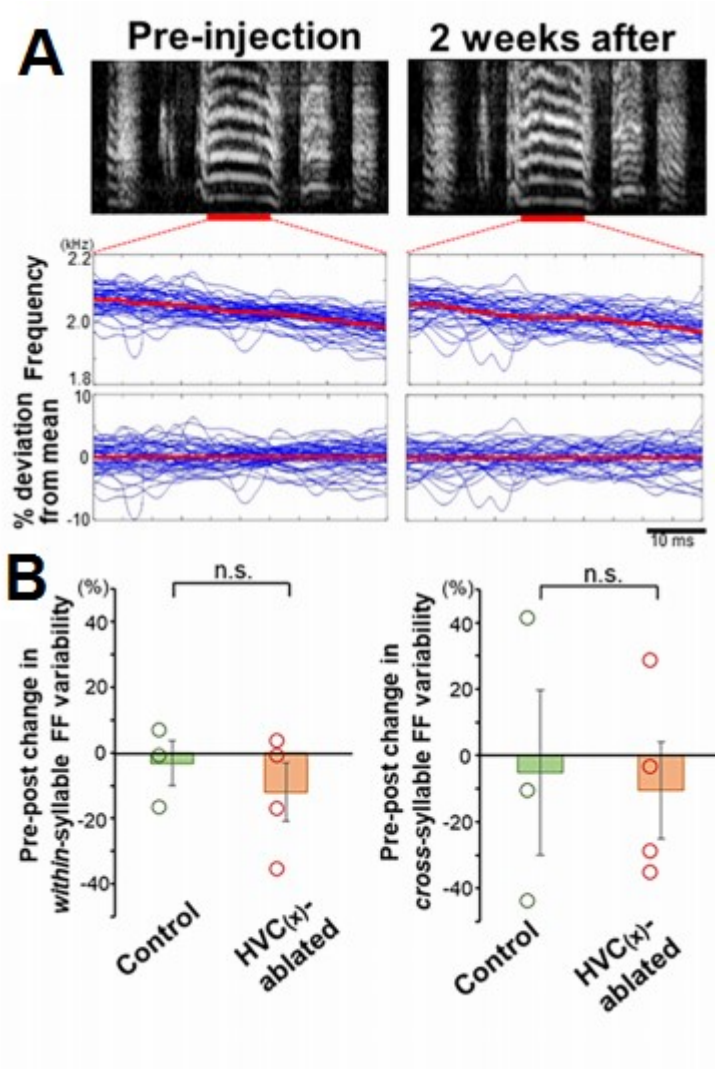
A
Pre-injection
2 weeks after
(kHz)
2.2
2.0
1.8
Frequency
10
0
-10
% deviation from mean
10 ms
B
n.s.
(%)
40
20
0
-20
-40
Pre-post change in within-syllable FF variability
Control
HVC(x)-ablated
n.s.
(%)
40
20
0
-20
-40
Pre-post change in cross-syllable FF variability
Control
HVC(x)-ablated

(A) Example of the fundamental frequency (FF) trajectory of a syllable in pre-injection (top left) and 2 weeks post-injection (top right) of songs from an $HVC_{(X)}$-ablated adult, expressed as raw frequency traces (middle) and percent deviation from the within-rendition mean (bottom). Blue and red lines indicate each rendition and the mean across renditions, respectively.

(B) Pre–post changes in within- (Wilcoxon's signed rank test: n.s., $p = 0.857$) and cross-rendition (Wilcoxon's signed rank test: n.s., $p = 1$) syllable variability in FF between control and $HVC_{(X)}$-ablated birds. Mean +SEM for all graphs.

Figure R-11

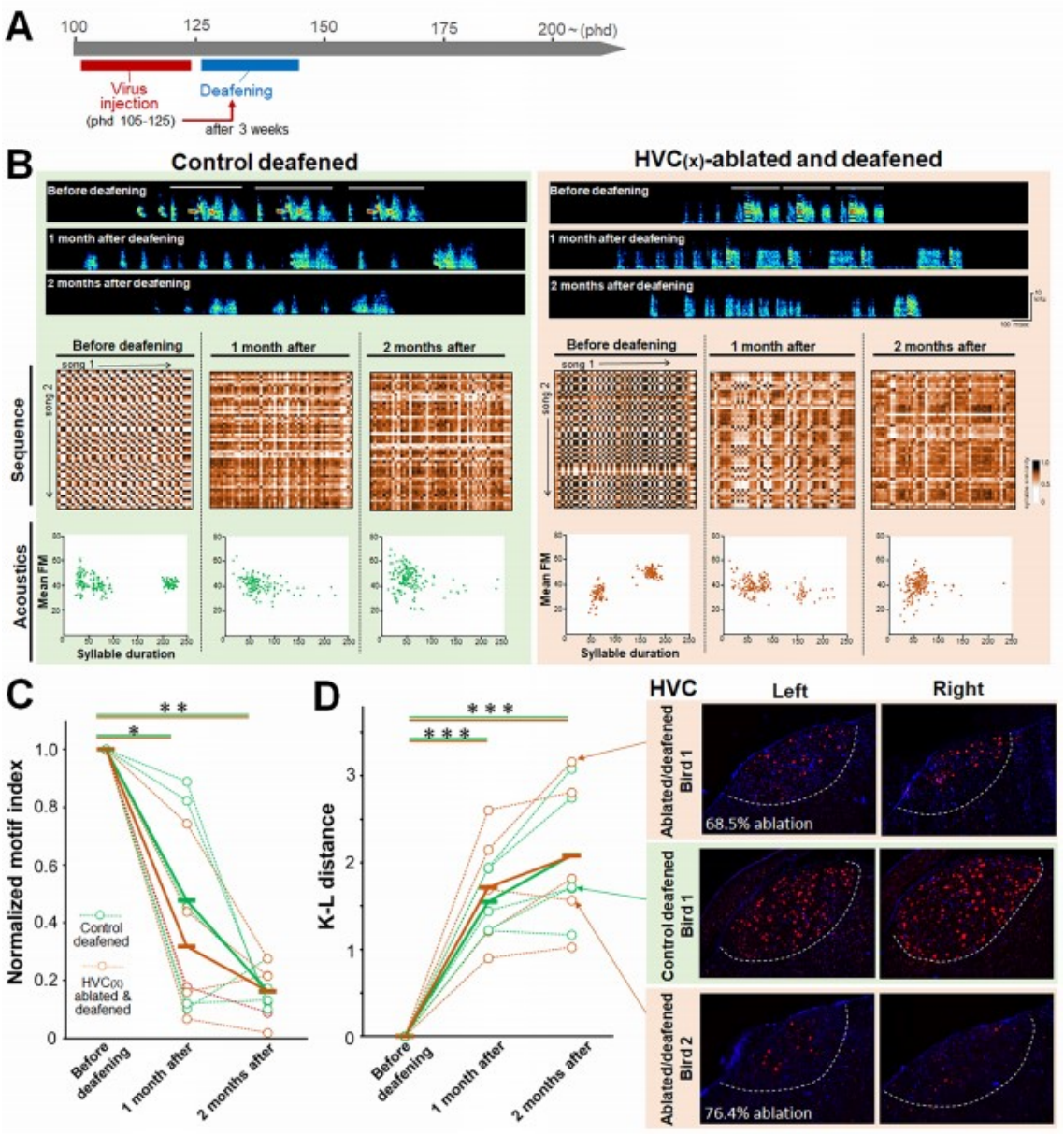
A
100
125
150
175
200 ~ (phd)
Virus injection (phd 105-125)
Deafening
after 3 weeks
B
Control deafened
HVC(x)-ablated and deafened
Before deafening
1 month after deafening
2 months after deafening
Before deafening
1 month after
2 months after
Sequence
Acoustics
Mean FM
Syllable duration
C
Normalized motif index
Control deafened
HVC(x) ablated & deafened
Before deafening
1 month after
2 months after
D
K-L distance
HVC
Left
Right
Ablated/deafened Bird 1
68.5% ablation
Control deafened Bird 1
Ablated/deafened Bird 2
76.4% ablation

(A) Timeline of $HVC_{(X)}$ ablation and deafening in the adult stage.

(B) Deafening-induced degradation of the syllable sequence and acoustics in a control (green background) and $HVC_{(X)}$-ablated (brown background) adult birds.

(C Strong effect of deafening on species-specific song pattern degradation as calculated by the SSM methods (n = 5 for each group; Wilcoxon's signed rank test: $p = 0.00016$). No difference could be found between control and $HVC_{(X)}$-ablated birds at 2 months after deafening (Wilcoxon's signed rank test: n.s., $p = 0.841$). Green and brown lines represent control and $HVC_{(X)}$-ablated birds, respectively. Dotted- and solid lines represent individual and average values, respectively.

(D) (Left) Strong effect of deafening on acoustic degradation as calculated by the K–L divergence (n = 5 for each group; Wilcoxon's signed rank test: $p = 0.00001$). There is no difference, however, between control and $HVC_{(X)}$-ablated birds at 2 months after deafening (Wilcoxon's signed rank test: n.s., $p = 1$). (Right) Remaining $HVC_{(X)}$ neurons in three representative birds (a control and two $HVC_{(X)}$-ablated birds), visualized by NTS (red) and DAPI (blue). White dotted lines represent the border of HVC.

Discussion

The results of $HVC_{(X)}$ neuron ablation in juveniles are consistent, at least partially, with those expected from the "AFP as a reinforcement learning module" model, where $HVC_{(X)}$ time-locked input would be used as a "temporal context" information source (**Figure I-4**). Partial removal of $HVC_{(X)}$ input could cause an inability to either reduce AFP-driven variability impeding the detailed refinement of syllable acoustics needed to match the current song to the tutor song through reinforcement learning, causing a reduction in the acoustic similarity to tutor (**Figure R-6*B***). Defects in sequence learning arising from partially missing time-locked information can also cause song sequence learning disruptions, shown in the inability to learn the species-specific motif pattern (**Figure R-8**).

However, alternative mechanisms unrelated to reinforcement learning models may also lie behind the effects of $HVC_{(X)}$ neuron ablation on the learning of syllable acoustics and song sequence. An additional explanation of $HVC_{(X)}$ effects on song sequence may lie in the recent finding of a pathway indirectly linking AFP nucleus Area X to nucleus HVC through the A12 midbrain area in adult zebra finches (Hamaguchi and Mooney, 2012). Activity flowing from an Area X with a reduced "temporal context" input due to $HVC_{(X)}$ ablation could in theory affect syllable transitions, as manipulations of this midbrain to HVC pathway cause an increase in sequence variability. Additionally, in a manner similar to mammalian cortical projection neurons (Kawaguchi, 2017), $HVC_{(X)}$ neurons also connect extensively inside the HVC (Mooney and Prather, 2005). A potentially abnormal HVC connectivity caused by the removal of $HVC_{(X)}$ neurons may be the cause of sequence deficits, as well as the known support functions of $HVC_{(X)}$

neurons towards $HVC_{(RA)}$ neurons. A previous study using laser ablation to kill $HVC_{(X)}$ neurons found that the number of newborn $HVC_{(RA)}$ neurons added to nucleus RA increased after $HVC_{(X)}$ neuron ablation in juvenile zebra finches, potentially causing an imbalance in HVC activity or connectivity (Scharff et al., 2000). These same newborn $HVC_{(RA)}$ neurons use $HVC_{(X)}$ neurons as a guide for their correct migration inside HVC (Scott et al., 2012). Furthermore, the production of retinoic acid in HVC is necessary for the correct learning of syllable acoustics and inter-syllable gaps, with the retinoic acid synthesizing enzyme's RNA being only transcribed in $HVC_{(X)}$ neurons (Denisenko-Nehrbass et al., 2000; Roeske et al., 2014). All these additional functions need to be considered when interpreting the results of $HVC_{(X)}$ ablation in song learning.

The results of $HVC_{(X)}$ neuron ablation in adult birds were different from those of $HVC_{(X)}$ neuron ablation in juveniles. A previous study reported no general changes in adult song after an $HVC_{(X)}$ neuron ablation of roughly 60% by laser (Scharff et al., 2000). This previous finding was confirmed and extended by fine acoustic and sequence analysis of the song of $HVC_{(X)}$-ablated birds (**Figure R-9**). As a new result, no change in Area X-generated vocal fluctuations could be detected either (**Figure R-10**). Secondly, no effect of $HVC_{(X)}$ neuron ablation was found on deafening-induced degradation, at the sequence or acoustic levels (**Figure R-11**). Taken together, these results indicate that ablation of a major part of the $HVC_{(X)}$ population, over 70% of the population on average (**Figure R-3**), has no effect on AFP-generated adult song plasticity.

A similar level of $HVC_{(X)}$ neuron ablation (mean ablation of 73%) caused striking defects in juvenile learning but no difference in the songs of $HVC_{(X)}$-ablated adult birds.

This difference between juvenile and adult ablations suggests that if there is any function of $HVC_{(X)}$ neurons in adult vocal plasticity, it is greatly reduced or residual when compared to its effects on juvenile song learning. Recent studies focusing on the mechanisms of adult song plasticity have identified a set of brain areas involved in the evaluation of auditory input and motor output to bias the AFP, and found that at least one of these areas, the ventral pallidum, receives input time-locked to song from nucleus uvaeformis (Uva) (Chen et al., 2019). The limited extent of adult song plasticity may require a less complete temporal code, thus being unaffected by major but still incomplete $HVC_{(X)}$ neuron ablation. Alternatively, the AFP in adulthood may be able to produce vocal fluctuation independently from $HVC_{(X)}$ input or by using timing information from other areas such as Uva.

This study achieved ablation percentages of $HVC_{(X)}$ neuron numbers around 75%, comparable to that of previously published cell-specific ablation studies in songbirds. From laser ablation of $HVC_{(X)}$ neurons achieving 60% of ablation (Scharff et al., 2000) to the roughly 60% of cell ablation obtained using other viral combinations with Cre and FLEx-flanked toxins on different cell types (Hisey et al., 2018; Roberts et al., 2017). In contrast, injection of AAVs containing FLEx-flanked caspase sequences into transgenic mice expressing Cre in specific cell types can cause cell ablations of over 90% (Yang et al., 2013). Unlike mammals and like previously reported studies in songbirds, the main drawback of the viral combination method in this study is the inability to completely ablate the $HVC_{(X)}$ target population, while its main strong point is its cell-specificity. This caveat needs to be considered when $HVC_{(X)}$ ablation shows no apparent effect on behavior, as this might be caused by the intact $HVC_{(X)}$ cells being sufficient to maintain the behavior. Using the Cre-FLEx toxin combined technique and

considering its limitations, an investigation into the role of $HVC_{(X)}$ projection neurons in both juvenile learning and adult songbirds became possible.

Furthermore, $HVC_{(X)}$ neurons have different functions besides their projection to Area X. New procedures will be needed to elucidate the possibly multiple roles of $HVC_{(X)}$ input. One of these possible experiments may involve using the Cre-FLEx system to cell-specifically express optogenetic effectors into $HVC_{(X)}$ neurons and use area-specific illumination that would either activate or suppress synaptic activity of the $HVC_{(X)}$ axons. Optogenetics would allow the targeting of axons projecting to a specific area during development, for instance, suppressing only the $HVC_{(X)}$ axons leading Area X but not those into HVC to separate the possibly different effects of $HVC_{(X)}$ input into these areas. Alternatively, an optogenetic short-pulse stimulation regime using activating rhodopsins could be used on $HVC_{(X)}$ input into Area X to disrupt time-locked bursts, as this regime has previously been used in the zebra finch (Roberts et al., 2012). These region-specific manipulations during development could help solve the question whether the effects of $HVC_{(X)}$ manipulation on vocal learning are specific to their effect on AFP targets or intra-HVC connections. In the case that the effects of $HVC_{(X)}$ neuron ablation on acoustics and sequence are caused by $HVC_{(X)}$ input into Area X, the effects on song should only be present when specifically inhibiting Area X-innervating axons. Alternatively, acoustics and sequence learning should only be affected when specifically stimulating $HVC_{(X)}$ input into Area X in a completely different pattern than the natural one.

As a more general application to the findings of this study to neuroscience, the lack of observable effects of $HVC_{(X)}$ ablation on already learned song is similar to studies in

mammals. In rodents where the motor cortex was ablated after learning of a skilled motor task, no effects were found on task execution after ablation (Kawai et al., 2015). The rodent study contrasts with the situation in humans, where lesions of speech-related motor cortices lead to speech apraxia, as well as non-cell specific lesion of HVC in songbirds, which completely abolishes adult song (Graff-Radford et al., 2014; Moser et al., 2016; Aronov et al., 2008). These paradoxical results regarding the involvement of cortical input on different skilled motor tasks may be explained partly by this study's findings. This may be caused by some tasks relying on different neuron populations that are mixed in mammalian cortices but show different contributions to the maintenance of learned skills, therefore abolishing both learning and maintenance in some cases but not others. Different contributions by mixed neuron populations of motor cortices may lie behind the observation that some previously learned motor skills, such as lever pulling in rats, are resistant to motor cortex ablation while others are lost.

Summing the results of this study up, $HVC_{(X)}$ neuron ablations of a similar extent to those that caused highly aberrant song learning in juveniles failed to cause any measurable dysfunction in song production, fluctuation or deafening-induced degradation when performed in adult zebra finches. New approaches will be needed to confirm or refute a putative lack of $HVC_{(X)}$ neuron role in adult song plasticity, such as complete $HVC_{(X)}$ neuron ablation by using transgenic songbirds or performing pitch shift experiments in $HVC_{(X)}$-ablated adults. Taking the limitations of the current experimental methods into account, $HVC_{(X)}$ neuron function appears to be critical for juvenile song learning but largely dispensable for adult song maintenance.

Acknowledgements

I want to show my deep gratitude and respect towards my supervisor, Dr. Kazuhiro Wada, who helped me overcome many hurdles and guided me through this difficult yet rewarding path. This work was no pleasant trip, yet Wada-sensei never lost patience and always worked very hard and offered guidance during all crucial points and times. He shall be remembered as a great mentor not just by me, but most likely by all his students. I learned the hard but treasure-ridden path from him, he showed what true scientific dedication looked like.

I thank the professors from the Behavior and Neuroscience department at Hokkaido University for their engaging talk and exemplar behavior towards all of the graduate and undergraduate students. I also want to thank all the professors who engaged with me during the progress reports to improve this work, as my co-PhD committee advisors Dr. Hiroto Ogawa and Dr. Toshiya Matsushima, as well as Dr. Makoto Mizunami.

I also wish to thank all the outside faculty and researchers who collaborated in bringing this work to life, such as: Dr. Satoshi Kojima, Dr. Daisuke Mizuguchi from the Korean Brain Research Institute, Dr. Kenta Kobayashi from the National Institute of Physiological Science, Dr. Kazuo Okanoya from Tokyo University and Dr. Haruo Okado from the Tokyo Metropolitan Institute for Medical Science.

This work would have been impossible to produce without the hard work of my lab colleagues, and as such I show them my gratitude and apologize for any inconveniences I caused them. These vital colleagues are Dr. Chinweike Norman Asogwa, Dr. Chihiro Mori, Dr. Shin Hayase and Dr. Noriyuki Touji as well as excellent graduate students as

Yukino Shibata, Yu Ji, Hongdi Wang, Azusa Sawai, Wu Xia, Rintarou Sugioka and Ippei Kojima. As well as the outstanding undergraduate students Yumeno Suzuki, Nasiba Afrin, Jun Ishigohoka and Yuto Nakagawa. A big thanks also to the serious and hard-working Keiko Sumida, who provided excellent and crucial bird care.

Last but not least, I want to thank Marie-Elène Valpuesta and Manuel Sánchez, as well as Yara Ferrero for their unwavering patience and support.

References

Abe K, Matsui S, Watanabe D. 2015 Transgenic songbirds with suppressed or enhanced activity of CREB transcription factor. Proceedings of the National Academy of Sciences U S A. Jun 16;112(24):7599-604.

Agate R. J, Scott B. B, Haripal B, Lois C, Nottebohm F. 2009 Transgenic songbirds offer an opportunity to develop a genetic model for vocal learning. Proceedings of the National Academy of Sciences U S A. Oct 20;106(42):17963-7.

Ahmed B. Y, Chakravarthy S, Eggers R, Hermens W. T, Zhang JY, Niclou S. P, Levelt C, Sablitzky F, Anderson P. N, Lieberman A. R, Verhaagen J. 2004 Efficient delivery of Cre-recombinase to neurons in vivo and stable transduction of neurons using adeno-associated and lentiviral vectors. BMC Neurosci. Jan 30;5:4.

Ali F, Otchy T. M, Pehlevan C, Fantana A. L, Burak Y, Ölveczky B. P. 2013 The basal ganglia is necessary for learning spectral, but not temporal, features of birdsong. Neuron. Oct 16;80(2):494-506.

Barnes T. D, Kubota Y, Hu D, Jin D. Z, Graybiel A. M. 2005 Activity of striatal neurons reflects dynamic encoding and recoding of procedural memories. Nature. Oct 20;437(7062):1158-61.

Bottjer S. W, Miesner E. A, Arnold A. P. 1984 Forebrain lesions disrupt development but not maintenance of song in passerine birds. Science. May 25;224(4651):901-3.

Bouabe H and Okkenhaum K. 2013 Gene Targeting in Mice: a Review. Methods in Molecular Biology; 1064: 315–336.

Branda CS, Dymecki SM. 2004 Talking about a revolution: the impact of site-specific recombinases on genetic analyses in mice. Developmental Cell 6:7–28.

Brenowitz E. A, Margoliash D, Nordeen K. W. 1997 An introduction to birdsong and the avian song system. Journal of Neurobiology. Nov;33(5):495-500.

Chakraborty M, Walløe S, Nedergaard S, Fridel E. E, Dabelsteen T, Pakkenberg B, Bertelsen M.F, Dorrestein G. M, Brauth S. E, Durand S. E, Jarvis E. D. 2015 Core and Shell Song Systems Unique to the Parrot Brain. PLoS One. Jun 24;10(6):e0118496.

Chen R, Puzerey P. A, Roeser A. C, Riccelli T. E, Podury A, Maher K, Farhang A. R, Goldberg J. H. 2019 Songbird Ventral Pallidum Sends Diverse Performance Error Signals to Dopaminergic Midbrain. Neuron. July 17;103(2):266-276.e4.

Denisenko-Nehrbass N. I, Jarvis E, Scharff C, Nottebohm F, Mello C. V. 2000 Site-Specific Retinoic Acid Production in the Brain of Adult Songbirds. Neuron. Aug;27(2):359-70.

Doupe A. J and Kuhl P. K. 1999 Birdsong and human speech: common themes and mechanisms. Annual Reviews Neuroscience. 1999;22:567-631.

Doya K., Sejnowski T.J. 1998 A Computational Model of Birdsong Learning by Auditory Experience and Auditory Feedback. In: Poon P. W. F., Brugge J. F. (eds) Central Auditory Processing and Neural Modeling. Springer, Boston, MA

Dutar P, Vu H. M, Perkel D. J. 1998 Multiple cell types distinguished by physiological, pharmacological, and anatomic properties in nucleus HVc of the adult zebra finch. Journal of Neurophysiology. Oct;80(4):1828-38.

Fee M.S, Goldberg J.H. 2011 A hypothesis for basal ganglia-dependent reinforcement learning in the songbird. Neuroscience. Dec 15;198:152-70.

Feng Y, Xiao Y, Yan Y, Max L. 2018 Adaptation in Mandarin tone production with pitch-shifted auditory feedback: Influence of tonal contrast requirements. Lang Cogn Neurosci. 2018;33(6):734-749.

Fujii N, Graybiel AM. 2003 Representation of action sequence boundaries by macaque prefrontal cortical neurons. Science. Aug 29;301(5637):1246-9.

Fukushima M, Margoliash D. 2015 The effects of delayed auditory feedback revealed by bone conduction microphone in adult zebra finches. Scientific Reports. Mar 5;5:8800.

Gadagkar V, Puzerey P. A, Chen R, Baird-Daniel E, Farhang A. R, Goldberg J. H. 2016 Dopamine neurons encode performance error in singing birds. Science. Dec 9;354(6317):1278-1282.

Garr E. 2019 Contributions of the basal ganglia to action sequence learning and performance. Neurosci Biobehav Rev. December;107:279-295.

Garst-Orozco J, Babadi B, Ölveczky B. P. 2014 A neural circuit mechanism for regulating vocal variability during song learning in zebra finches. Elife. Dec 15;3:e03697.

Graff-Radford J, Jones D. T, Strand EA, Rabinstein A. A, Duffy J. R, Josephs K. A. 2014 The neuroanatomy of pure apraxia of speech in stroke. Brain Lang. Feb;129:43-6.

Hahnloser R. H, Kozhevnikov A. A, Fee M. S. 2002 An ultra-sparse code underlies the generation of neural sequences in a songbird. Nature. Sep 5;419(6902):65-70.

Hamaguchi K. and Mooney R. 2012 Recurrent interactions between the input and output of a songbird cortico-basal ganglia pathway are implicated in vocal sequence variability. J Neurosci. Aug 22;32(34):11671-87.

Hamaguchi K, Tschida K. A, Yoon I, Donald B. R, Mooney R. 2014 Auditory synapses to song premotor neurons are gated off during vocalization in zebra finches. eLife 3:e01833.

Hikosaka O, Nakamura K, Sakai K, Nakahara H. 2002 Central mechanisms of motor skill learning. Current Opinion in Neurobiology. Apr;12(2):217-22.

Hisey E, Kearney MG, Mooney R. 2018 A common neural circuit mechanism for internally guided and externally reinforced forms of motor learning. Nature Neuroscience. Apr;21(4):589-597.

Horita H, Wada K, Jarvis E. D. 2008 Early onset of deafening-induced song deterioration and differential requirements of the pallial-basal ganglia vocal pathway. Eur J Neurosci. Dec;28(12):2519-32.

Huang Z. J and Zeng H. 2013 Genetic approaches to neural circuits in the mouse. Annual Reviews Neuroscience. Jul 8;36:183-215.

Imai R, Sawai A, Hayase S, Furukawa H, Asogwa CN, Sanchez M, Wang H, Mori C, Wada K. 2016 A quantitative method for analyzing species-specific vocal sequence pattern and its developmental dynamics. Journal of Neuroscience Methods. Sep 15;271:25-33.

Jarvis E. D. 2004 Learned birdsong and the neurobiology of human language. Annals New York Academy of Sciences. Jun;1016:749-77.

Jin X and Costa R.M. 2010 Start/Stop Signals Emerge in Nigrostriatal Circuits during Sequence Learning. Nature. Jul 22;466(7305):457-62.

Kageyama A, Kusano I, Tamura T, Oda T, Muramatsu T. 2002 Comparison of the apoptosis-inducing abilities of various protein synthesis inhibitors in U937 cells. Biosci Biotechnol Biochem. Apr;66(4):835-9.

Kao M. H, Doupe A. J, Brainard M. S. 2005 Contributions of an avian basal ganglia-forebrain circuit to real-time modulation of song. Nature. Feb 10;433(7026):638-43.

Kaspar B. K, Vissel B, Bengoechea T, Crone S, Randolph-Moore L, Muller R, Brandon E. P, Schaffer D, Verma I. M, Lee K. F, Heinemann S. F, Gage FH. 2002a Adeno-associated virus effectively mediates conditional gene modification in the brain. Proc Natl Acad Sci U S A. Feb 19;99(4):2320-5.

Kaspar B. K, Erickson D, Schaffer D, Hinh L, Gage F. H, Peterson DA 2002b Targeted retrograde gene delivery for neuronal protection. Molecular Therapy. Jan; 5(1):50-6.

Kawaguchi Y. 2017 Pyramidal Cell Subtypes and Their Synaptic Connections in Layer 5 of Rat Frontal Cortex. Cerebral Cortex, Volume 27, Issue 12, December, Pages 5755–5771

Kearney M. G, Warren T. L, Hisey E, Qi J, Mooney R. 2019 Discrete Evaluative and Premotor Circuits Enable Vocal Learning in Songbirds. Neuron. Nov 6;104(3):559-575.e6.

Kojima S, Kao M. H, Doupe A. J. 2013 Task-related "cortical" bursting depends critically on basal ganglia input and is linked to vocal plasticity. Proc Natl Acad Sci U S A. Mar 19;110(12):4756-61.

Kojima S, Kao M.H, Doupe A. J, Brainard M. S. 2018 The Avian Basal Ganglia Are a Source of Rapid Behavioral Variation That Enables Vocal Motor Exploration. Journal of Neuroscience. Nov 7;38(45):9635-9647.

Komatsu N, Oda T, Muramatsu T. 1998 Involvement of both caspase-like proteases and serine proteases in apoptotic cell death induced by ricin, modeccin, diphtheria toxin, and pseudomonas toxin. Journal of Biochemistry. Nov;124(5):1038-44.

Konishi M. 1965 Effects of deafening on song development in American robins and black-headed grosbeaks. Z Tierpsychol. Aug;22(5):584-99.

Koralek A. C, Jin X, Long J. D 2nd, Costa R. M, Carmena J.M. 2012 Corticostriatal plasticity is necessary for learning intentional neuroprosthetic skills. Nature. Mar 4;483(7389):331-5.

Kornysheva K. 2016 Encoding Temporal Features of Skilled Movements-What, Whether and How? Adv Exp Med Biol. 2016;957:35-54.

Kozhevnikov A.A and Fee M. S. 2007 Singing-related activity of identified HVC neurons in the zebra finch. Journal of Neurophysiology. Jun;97(6):4271-83.

Kroodsma D. E. and Konishi M. 1991 A suboscine bird (eastern phoebe, Sayornis phoebe) develops normal song without auditory feedback. Animal Behaviour. Volume 42, Issue 3, September, Pages 477-487

Kubota M. and Taniguchi I. 1998 Electrophysiological characteristics of classes of neuron in the HVc of the zebra finch. Journal of Neurophysiology. Aug;80(2):914-23.

Leonardo A, Konishi M. 1999 Decrystallization of adult birdsong by perturbation of auditory feedback. Nature. Jun 3;399(6735):466-70.

Li Q, Ko H, Qian Z. M, Yan L.Y, Chan D.C.W, Arbuthnott G, Ke Y, Yung W.H. 2017 Refinement of learned skilled movement representation in motor cortex deep output layer. Nature Communications. Jun 9;8:15834.

Liu H, Wang E. Q, Chen Z, Liu P, Larson C. R, Huang D. 2010 Effect of tonal native language on voice fundamental frequency responses to pitch feedback perturbations during sustained vocalizations. Journal of the Acoustic Society America. Dec;128(6):3739-46.

Liu W. C, Wada K, Jarvis E. D, Nottebohm F. 2013 Rudimentary substrates for vocal learning in a suboscine. Nature Communications. 2013;4:2082.

Lombardino A. J. and Nottebohm F. 2000 Age at Deafening Affects the Stability of Learned Song in Adult Male Zebra Finches. Journal of Neuroscience 1 July, 20 (13) 5054-5064

Long M. A, Jin D. Z, Fee M. S. 2010 Support for a synaptic chain model of neuronal sequence generation. Nature. Nov 18;468(7322):394-9.

Luo M, Ding L, Perkel D. J. 2001 An avian basal ganglia pathway essential for vocal learning forms a closed topographic loop. J Neurosci. Sep 1;21(17):6836-45.

Lynch G. F, Okubo T. S, Hanuschkin A, Hahnloser R. H, Fee MS. 2016 Rhythmic Continuous-Time Coding in the Songbird Analog of Vocal Motor Cortex. Neuron. May 18;90(4):877-92.

Madeo G, Martella G, Schirinzi T, Ponterio G, Shen J, Bonsi P, Pisani A. 2012 Aberrant striatal synaptic plasticity in monogenic parkinsonisms. Neuroscience. Jun 1;211:126-35.

Madisen L, Garner A. R, Shimaoka D, Chuong A. S, Klapoetke N. C, Li L, van der Bourg A, Niino Y, Egolf L, Monetti C, Gu H, Mills M, Cheng A, Tasic B, Nguyen T. N, Sunkin S. M, Benucci A, Nagy A, Miyawaki A, Helmchen F, Empson R. M, Knöpfel T, Boyden E.S, Reid R.C, Carandini M, Zeng H. 2015 Transgenic mice for intersectional targeting of neural sensors and effectors with high specificity and performance. Neuron. Mar 4;85(5):942-58.

Mandelblat-Cerf Y, Las L, Denisenko N, Fee M. S. 2014 A role for descending auditory cortical projections in songbird vocal learning. Elife. Jun 16;3.

Marler P. 1970 Birdsong and speech development: could there be parallels? American Scientist. Nov-Dec;58(6):669-73

McCarty D. M, Monahan P. E, Samulski R. J. 2001 Self-complementary recombinant adeno-associated virus (scAAV) vectors promote efficient transduction independently of DNA synthesis. Gene Therapy. Aug;8(16):1248-54.

Mehaffey W. H and Doupe A. J. 2015 Naturalistic stimulation drives opposing heterosynaptic plasticity at two inputs to songbird cortex. Nature Neuroscience. Sep;18(9):1272-80.

Mooney R. and Prather J. F. 2005 The HVC microcircuit: the synaptic basis for interactions between song motor and vocal plasticity pathways. Journal of Neuroscience. Feb 23;25(8):1952-64.

Moser D, Basilakos A, Fillmore P, Fridriksson J. 2016 Brain damage associated with apraxia of speech: evidence from case studies. Neurocase. Aug;22(4):346-56.

Nordeen K. W. and Nordeen E. J. 2010 Deafening-Induced Vocal Deterioration in Adult Songbirds Is Reversed by Disrupting a Basal Ganglia-Forebrain Circuit. Journal of Neuroscience 26 May, 30 (21) 7392-7400

Okubo T. S, Mackevicius E. L, Payne H. L, Lynch G. F, Fee M. S. 2015 Growth and splitting of neural sequences in songbird vocal development. Nature. Dec 17;528(7582):352-7.

Orban P. C, Chui D, Marth J. D. 1992 Tissue- and site-specific DNA recombination in transgenic mice. Proceedings of the National Academy of Sciences of the United States of America.1992;89:6861–6865.

Patricelli, G. L. and Blickley, J. L. 2006. Avian Communication in Urban Noise: Causes and Consequences of Vocal Adjustment. The Auk, 123(3), 639-649.

Picardo M. A, Merel J, Katlowitz K. A, Vallentin D, Okobi D. E, Benezra S. E, Clary R. C, Pnevmatikakis E. A, Paninski L, Long M. A. 2016 Population-Level Representation of a Temporal Sequence Underlying Song Production in the Zebra Finch. Neuron. May 18;90(4):866-76.

Roberts T. F, Gobes S. M, Murugan M, Ölveczky B. P, Mooney R. 2012 Motor circuits are required to encode a sensory model for imitative learning. Nature Neuroscience. October;15(10):1454-9.

Roberts T. F, Hisey E, Tanaka M, Kearney M. G, Chattree G, Yang C. F, Shah N. M, Mooney R. 2017 Identification of a motor-to-auditory pathway important for vocal learning. Nature Neuroscience. Jul;20(7):978-986.

Rock C, Zurita H, Wilson C, Apicella A. J. 2016 An inhibitory corticostriatal pathway. Elife. May 9;5. pii: e15890.

Roeske T. C, Scharff C, Olson C. R, Nshdejan A, Mello C. V. 2014 Long-distance retinoid signaling in the zebra finch brain. PLoS One. Nov 13;9(11):e111722.

Rothermel M, Brunert D, Zabawa C, Díaz-Quesada M, Wachowiak M. 2013 Transgene expression in target-defined neuron populations mediated by retrograde infection with adeno-associated viral vectors. Journal of Neuroscience. Sep 18; 33(38):15195-206.

Scharff C, Kirn J. R, Grossman M, Macklis J. D, Nottebohm F. 2000 Targeted neuronal death affects neuronal replacement and vocal behavior in adult songbirds. Neuron. Feb;25(2):481-92.

Scharff C, Nottebohm F. 1991 A comparative study of the behavioral deficits following lesions of various parts of the zebra finch song system: implications for vocal learning. Journal of Neuroscience. Sep;11(9):2896-913.

Scott B. B, Gardner T, Ji N, Fee M. S, Lois C. 2012 Wandering neuronal migration in the postnatal vertebrate forebrain. Journal of Neuroscience. Jan 25;32(4):1436-46.

Gong S, Doughty M, Harbaugh C. R, Cummins A, Hatten M. E, Heintz N, Gerfen C. R. 2007 Targeting Cre Recombinase to Specific Neuron Populations with Bacterial Artificial Chromosome Constructs. Journal of Neuroscience 27 (37) 9817-9823

Shadmehr R. and Krakauer J. W. 2008 A computational neuroanatomy for motor control. Experimental Brain Research. March;185(3):359-81.

Slabbekoorn H. and Ripmeester E. A. 2008 Birdsong and anthropogenic noise: implications and applications for conservation. Molecular Ecology. Jan;17(1):72-83.

Sober S. J. and Brainard M. S. 2009 Adult birdsong is actively maintained by error correction. Nature Neuroscience. Jul;12(7):927-31.

Sohrabji F, Nordeen E. J, Nordeen K. W. 1990 Selective impairment of song learning following lesions of a forebrain nucleus in the juvenile zebra finch. Behavioral and Neural Biology 53, 51–63

Solis M. M, Brainard M. S, Hessler N. A, Doupe A. J. 2000 Song selectivity and sensorimotor signals in vocal learning and production. Proceedings of the National Academy of Sciences. Oct 24;97(22):11836-42.

Stefanova E. D, Kostic V.S, Ziropadja L, Markovic M, Ocic G. G. 2000 Visuomotor skill learning on serial reaction time task in patients with early Parkinson's disease. Movement Disorders. Nov;15(6):1095-103.

Striedter G. F. 1994 The vocal control pathways in budgerigars differ from those in songbirds. Journal of Comparative Neurology. May 1;343(1):35-56.

Takahashi D. Y, Liao D. A, Ghazanfar A. A. 2017 Vocal Learning via Social Reinforcement by Infant Marmoset Monkeys. Current Biology. Jun 19;27(12):1844-1852.e6.

Taniguchi H, He M, Wu P, Kim S, Paik R, et al. 2011. A resource of Cre driver lines for genetic targeting of GABAergic neurons in cerebral cortex. Neuron 71:995–1013

Tanji J. 2001 Sequential organization of multiple movements: involvement of cortical motor areas. Annual Reviews Neuroscience. 2001;24:631-51.

Teşileanu T, Ölveczky B, Balasubramanian V. 2017 Rules and mechanisms for efficient two-stage learning in neural circuits. Elife. Apr 4;6. pii: e20944.

Turner R. S. and DeLong M. R. 2000 Corticostriatal activity in primary motor cortex of the macaque. Journal of Neuroscience. Sep 15;20(18):7096-108.

Vallentin D. and Long M. A. 2015 Motor origin of precise synaptic inputs onto forebrain neurons driving a skilled behavior. J Neurosci. January 7;35(1):299-307

Vicario D. S. and Nottebohm F. 1988 Organization of the zebra finch song control system: I. Representation of syringeal muscles in the hypoglossal nucleus. Journal of Comparative Neurology. May 15;271(3):346-54.

Warre R, Thiele S, Talwar S, Kamal M, Johnston T. H, Wang S, Lam D, Lo C, Khademullah C.S, Perera G, Reyes G, Sun X. S, Brotchie JM, Nash J. E. 2011 Altered function of glutamatergic cortico-striatal synapses causes output pathway abnormalities in a chronic model of parkinsonism. Neurobiology of Disease. Mar;41(3):591-604

Wild J. M. 1993 Descending projections of the songbird nucleus robustus archistriatalis. Journal of Comparative Neurology. Dec 8;338(2):225-41.

Willingham D. B and Koroshetz W. J.1993 Evidence for dissociable motor skills in Huntington's disease patients. Psychobiology. September, Volume 21, Issue 3, pp 173–182

Xiao L, Chattree G, Oscos F. G, Cao M, Wanat M. J, Roberts T. F. 2018 A Basal Ganglia Circuit Sufficient to Guide Birdsong Learning. Neuron. Apr 4;98(1):208-221.e5.

Yang C. F, Chiang M. C, Gray D. C, Prabhakaran M, Alvarado M, Juntti SA, Unger E. K, Wells J. A, Shah N. M. 2013 Sexually dimorphic neurons in the ventromedial hypothalamus govern mating in both sexes and aggression in males. Cell. May 9;153(4):896-909.

Main Publication

Sánchez-Valpuesta M, Suzuki Y, Shibata Y, Toji N, Ji Y, Afrin N, Asogwa CN, Kojima I, Mizuguchi D, Kojima S, Okanoya K, Okado H, Kobayashi K, Wada K. (2019) Corticobasal ganglia projecting neurons are required for juvenile vocal learning but not for adult vocal plasticity in songbirds. *Proceedings of the National Academy of Sciences USA*. ~~November 5;~~116(45): 22833-22843.

List of other publications

Imai R., Sawai A., Hayase S., Furukawa H., Asogwa C. N., **Sánchez M**., Wang H. and Wada K. (2016). A quantitative method for analyzing species-specific vocal sequence pattern and its developmental dynamics. *Journal of Neuroscience Methods*, 271: 25-33.

Merullo D. P., Asogwa C. N., **Sánchez-Valpuesta M**., Hayase S., Pattnaik B. R., Wada K. and Riters L. V. (2018). Neurotensin and Neurotensin Receptor 1 mRNA Expression in Song-Control Regions Changes During Development in Male Zebra Finches. *Developmental Neurobiology*, 78: 671 – 686.

Asogwa C. N., Mori C., **Sánchez-Valpuesta M**., Hayase, S and Wada K. (2018). Inter- and intra-species differences in muscarinic acetylcholine receptor expression in the neural pathways for learned vocalization in songbirds. *Journal of Comparative Neurology* December 1;526(17):2856-2869.

Poster presentations

Asogwa, C. N., **Sánchez-Valpuesta M**., Hayase S., Mori C. and Wada K. (2017). Species-specificity and individual differences of muscarinic acetylcholine receptor expression in the song circuits. *Society for Neuroscience, Washington, DC, USA.* November 11-15, 2017.

Merullo D. P., Asogwa C. N., **Sánchez-Valpuesta M.**, Wada K. and Riters L. V. (2017). Neurotensin and neurotensin receptor 1 mRNA expression in song-control regions changes during development in male zebra finches. *Society for Neuroscience, Washington, DC, USA.* November 11-15, 2017.

Sánchez-Valpuesta M., Asogwa C. N. and Wada K. (2018). Cell-type specific investigation of corticostriatal neurons in motor skill learning. *Principles of Memory Dynamism Elucidated from a Diversity of Learning Systems, Toyama, Japan.* March 5-7, 2018.

Sánchez-Valpuesta M., Yukino S., Asogwa C. N., Kobayashi K. and Wada K. (2018). Cell-type specific investigation of corticostriatal premotor neurons in motor skill learning. *Society for Neuroscience, San Diego, CA, USA.* November 3-7, 2018.